Marine Physical Laboratory

Environmental Observations During the 1995 Adaptive Beach Monitoring Experiment

G. L. D'Spain, R. Shear, R. M. Olivera, J. J. Murray, W. S. Hodgkiss, W. A. Kuperman, and K. Melville

Supported by the
Chief of Naval Research
Contract N00014-93-D-0141 (DO#10)

19970204 005

MPL Technical Memorandum 446

MPL-U-79/95
October 1996

Approved for public release; distribution is unlimited.

University of California, San Diego
Scripps Institution of Oceanography

DTIC QUALITY INSPECTED 1

DISCLAIMER NOTICE

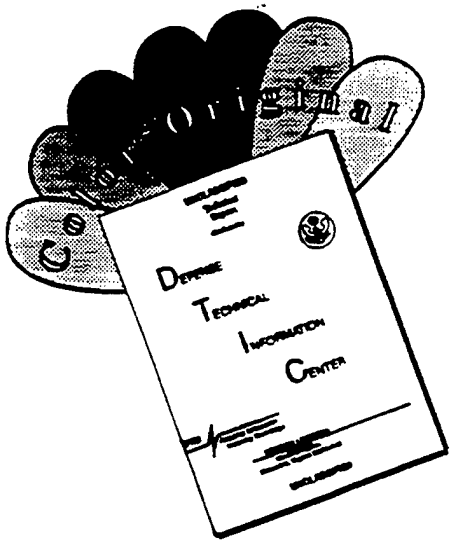

THIS DOCUMENT IS BEST QUALITY AVAILABLE. THE COPY FURNISHED TO DTIC CONTAINED A SIGNIFICANT NUMBER OF COLOR PAGES WHICH DO NOT REPRODUCE LEGIBLY ON BLACK AND WHITE MICROFICHE.

REPORT DOCUMENTATION PAGE

Form Approved OMB No. 0704-0188

Public reporing burden for this collection of information is estimated to average 1 hour per response, including the time for reviewing instructions, searching existing data sources, gathering and maintaining the data need ed, and completing and reviewing the collection of information. Send comments regarding this burden estimate or any other aspect of this collection of information, including suggestions for reducing this burden, to Washington Headquarters Services, Directorate for information Operations and Reports, 1215 Jefferson Davis Highway, Suite 1204, Arlington, VA 22202-4302, and to the Office of Management and Budget, Paperwork Reduction Project (0704-0188), Washington, DC 20503.

1. Agency Use Only (Leave Blank).

2. Report Date. October 1996

3. Report Type and Dates Covered. Technical Memorandum

4. Title and Subtitle.
Environmental Observations During the 1995 Adaptive Beach Monitoring Experiment

5. Funding Numbers.
N00014-93-D-0141
(DO#10)

Project No.
Task No.

6. Author(s).
G. L. D'Spain, R. Shear, R. M. Olivera, J. J. Murray, W. S. Hodgkiss, W. A. Kuperman, and K. Melville

7. Performing Monitoring Agency Names(s) and Address(es).
University of California, San Diego
Marine Physical Laboratory
Scripps Institution of Oceanography
San Diego, California 92152

8. Performing Organization Report Number.
MPL-U-79/95
MPL TM-446

9. Sponsoring/Monitoring Agency Name(s) and Address(es).
Chief of Naval Research
Department of the Navy
800 North Quincy Street
Arlington, VA 22217-5660
Code 321US

10. Sponsoring/Monitoring Agency Report Number.

11. Supplementary Notes.

12a. Distribution/Availability Statement.
Approved for public release; distribution is unlimited.

12b. Distribution Code.

13. Abstract (Maximum 200 words).

The Marine Physical Laboratory's Adaptive Beach Monitirong Pilot Experiment was conducted during the 8-week period from 24 April to 16 June 1995. Seismoacoustic, magnetic, electric, environmental, and other ancillary sensor systems were deployed both on the beach and in the near-shore waters off the Camp Pendleton Marine Base in Southern California. The purpose of this report is to present and discuss the environmental measurements made during the experiment. These environmental measurements include basic weather data, water sound speed, water depth, ocean surface wave activity, ocean currents, and traffic patterns along Highway 5.

14. Subject Terms.
environmental measurements, time series, sensor systems

15. Number of Pages. 46

16. Price Code.

17. Security Classification of Report.	18. Security Classification of This Page.	19. Security Classification of Abstract..	20. Limitation of Abstract.
Unclassified	Unclassified	Unclassified	None

ENVIRONMENTAL OBSERVATIONS during the 1995 ADAPTIVE BEACH MONITORING EXPERIMENT

G. L. D'Spain, R. Shear, R. M. Olivera, J. J. Murray,

W. S. Hodgkiss, W. A. Kuperman, and K. Melville

Marine Physical Laboratory,

Scripps Institution of Oceanography,

San Diego, CA 92152-6400

Abstract

The Marine Physical Laboratory's Adaptive Beach Monitoring Pilot Experiment was conducted during the 8-week period from 24 April to 16 June, 1995. Seismoacoustic, magnetic, electric, environmental, and other ancillary sensor systems were deployed both on the beach and in the near-shore waters of the Camp Pendleton Marine Base in Southern California. The purpose of this report is to present and discuss the environmental measurements made during the experiment. These environmental measurements include basic weather data, water sound speed, water depth, ocean surface wave activity, ocean currents, and traffic patterns along Highway 5.

The most apparent feature in the time series of the measurements is the predominance of the diurnal component of the variability. This observation has implications for data sampling schemes in future experiments. In addition, an increase in the daily average air temperature over the second half of the experiment correlates with an increase in sound speed at all water depths. Also, high ocean surface wave events fit into three categories: 1) short-period events that are correlated with increases in local winds and propagate predominantly in an easterly direction; 2)

short-period events that are not correlated with the local wind; and 3) long-period events that arise from deep-water swell propagating into the near-shore region. The long-period swell events travel mainly in a direction perpendicular to the shoreline, probably due to bottom refraction. However, they also typically have an upcoast component of propagation, most likely due to the presence of offshore islands that permit only southerly swell to arrive unimpeded. These long-period events have the greatest impact on ocean currents, biasing the flows towards the upcoast direction and at times giving rise to speeds exceeding 50 cm/sec. These conclusions were drawn by visual inspection of the time series. However, quantitative comparisons also can be made as illustrated by the coherence squared estimate between tide heights and north-bound Highway 5 vehicle counts. At diurnal periods, 90 percent of the variability in tide heights is linearly related to variations in the Highway 5 vehicle counts. Coherence squared estimates also can be used to measure the time delays of the tide height variations between pairs of stations along the coast.

INTRODUCTION

The Adaptive Beach Monitoring (ABM) Pilot Experiment was conducted by the Marine Physical Laboratory (MPL), Scripps Institution of Oceanography, during the 8-week period from 24 April to 16 June, 1995. Other participants included the Naval Command, Control, and Ocean Surveillance Center, RDT&E Division (NRaD/NCCOSC), the Naval Research Laboratory (NRL), the Applied Research Laboratory/Penn State University (ARL/PSU), and the Applied Research Laboratory/University of Texas at Austin (ARL/UT). Seismoacoustic, magnetic, electric, environmental, and other ancillary sensor systems were deployed both on the beach and in the near-shore waters of the Camp Pendleton Marine Base in Southern California. The section of the Camp Pendleton operations chart where most of the experiment was conducted is shown in Fig. 1. The purpose of this report is to present and discuss the environmental measurements made during the experiment. These environmental measurements characterize basic weather patterns, water sound speed, water depth, ocean surface wave activity, ocean currents, and traffic patterns along Highway 5 during the experiment.

A list of all the environmental and ancillary data collected during the experiment is given in the Appendix. The environmental sensor systems deployed on land and discussed in this report are 1) the 10-m weather station that measured wind speed and direction, air temperature, barometric pressure, and relative humidity; and 2) a traffic counter for both northbound and southbound traffic installed by the California Transportation Department (CalTrans) just north of the Oceanside exit on Highway 5. Not discussed are the data from two experimental, miniature weather stations installed with each of the two ARL/PSU land-based sensor pods. For measurement of the oceanographic properties of the near-shore environment over the course of the experiment, the following sensor systems were deployed: 1) two oceanography moorings about 20 m and 300 m from the shoreline; 2) a conductivity-temperature-depth (CTD) sensor; and 3) two cameras pointed at the surf zone and downcoast along the beach for day-time videocassette

recordings. The data from the video recordings and from the shallowest oceanography mooring, composed of a single bottom pressure sensor, are not presented; those from the deep mooring's bottom pressure sensor and two orthogonal, horizontal, electromagnetic current sensors, as well as the water sound speeds derived from the 15 CTD casts, are discussed.

In addition, environmental information were collected during a half-day of source tow operations on JD 161 (10 June). These data included: 1) water temperature at 5 m depth from the inclinometer package attached to the source tow cable; and 2) water depth from the shipboard fishfinder, both as a function of position along the source tow track. The time series and spatial variability of these measurements are presented.

To supplement the oceanographic data, two archival data sets were obtained: 1) ocean surface wave height data from Scripp's Coastal Data Information Program (CDIP) that were collected by a bottom pressure sensor array located offshore of the town of San Clemente, CA; and 2) tide heights from NOAA's tide stations at La Jolla and Santa Monica, CA.

In Section I, time series of the environmental measurements over the whole experiment are presented and compared. This is followed by the time series of the half-day measurements during the acoustic source tows on 10 June. Section II discusses the spatial variability of specific measurements; the CTD-derived sound speeds, the water temperature at 5 m, and the water depth. Finally, recommendations for the future major experiment in the ABM program are given.

I. TIME SERIES of the DATA and CORRELATIONS

To permit visual comparisons, the time series for environmental measurements covering the whole experiment were plotted on the same horizontal time scale. The scale starts at 12:00 GMT, JD 113 (Sunday, 23 April), and ends at 12:00 GMT, JD 169 (Sunday, June 18), covering a full 8-week period. The time frame over which seismoacoustic measurements were made is slightly smaller; from JD 115 (25 April) to JD 166 (15 June). The horizontal axis tick marks occur at

12:00 GMT (05:00 PDT) on even-numbered Julian days.

A. 10-m Weather Station Data

The 10-m weather station, owned and operated by the Center for Coastal Studies (CCS) at Scripps, was installed on the 3-m-tall bluff at the northern end of Red Beach, up-coast a few meters from the data acquisition van. It recorded the northerly and easterly components of wind, air temperature, atmospheric pressure and relative humidity. Both 1-min-averaged and 1-hour-averaged files were created during data downloading by CCS personnel. In the following three parts, the hourly averages are presented.

1. Winds

The northerly and easterly components of wind are converted into wind speed and direction. These quantities are plotted in the upper and lower panels of Fig. 2, respectively. Although the convention in meteorology is to report the direction the wind is coming *from*, the lower panel shows the direction the wind is blowing *to*, to be consistent with the oceanographic measurements presented later.

The most obvious feature of these time series is the diurnal nature of the variability. This variation is more spike-like than sinusoidal, with the high wind speed spikes typically occurring in the afternoon. The late night and early morning winds are light and typically blow to the SW. These diurnal effects are due to the lower heat capacity of land compared to that of the ocean.

The wind blows predominantly towards three directions -- to the E-NE (90° - 50°), to the SW (225°), and to the north. When the wind speed is high, the direction is to the E-NE. Since the normal to the coastline has a bearing of 51° [1], then strong winds typically have a down-coast component. The late-night and early morning hour winds move offshore, approximately perpendicular to the coastline.

Two wind events are notable. The first, occurring over the 1.5-day period on JD 124 - 126

(4 - 6 May), had sustained wind speeds around 8 m/sec. This event was accompanied by rain and forced a delay in deployment of the electric and magnetic sensor packages (EMP) until JD 128 (Mon, 8 May). The second event is the large wind speed spike that exceeds 9 m/sec on JD 160 (9 June). This event resulted in the cancellation of a sea trip on the Harbor Chief to refurbish the moored sonobuoy batteries.

2. Barometric Pressure

The plots of the barometric pressure and the relative humidity recorded by the 10-m weather station are shown in the upper and lower panels of Fig. 3, respectively. The barometric pressure measurements appear to be corrupted on and after JD 146 (Fri, 26 May), and those from the relative humidity sensor don't appear to be useful at any time. The cause(s) of these failures is unknown. Prior to JD 146, the barometric pressure time series show the omnipresent diurnal variability superimposed on fluctuations with a 3-6 day period. The large decrease in atmospheric pressure from JD 129-133 *may* be associated with the change in ocean surface wave significant wave angle (re Part C3 and Fig. 6) over this same period of time, although an association between the two measurement types is difficult to determine without a longer time series.

3. Air Temperature

The upper panel of Fig. 4 presents the hourly averages of air temperature over the course of the experiment. The predominant component of variability is diurnal. Examination of the longer period components reveals that the average daily temperature is approximately constant for the first half of the experiment, and then begins to rise steadily by 1-2° C starting about JD 146 (26 May), with the onset of summer. The two dips in the average daily air temperature in the first half of the experiment -- on JD 124-126 and on JD 133 -- are also times, or just follow times, of relatively high sustained winds.

B. Underwater Sound Speed

The lower panel of Fig. 4 presents the sound speed changes at five depths, 1 m, 5 m, 10 m, 15 m, and 20 m, as a function of time over the experiment. The sound speed data were calculated mostly from the 15 CTD (conductivity-temperature-depth) casts, with the values from multiple casts made on the same day averaged together. The one data point at 5 m depth on JD 161 (Sat, 10 June) was obtained from the inclinometer temperature sensor attached to the source tow cable.

Over the first two weeks of the experiment, the sound speed gradient between 10 and 15 m increased, due to a decrease in sound speed at depth. The mixed layer at the surface is at least 10 m thick. However, on JD 137 (Wed, 17 May), the sound speed in the mixed layer increased, followed shortly by a significant thinning of the mixed layer and a decrease in the sound speed gradient on JD 140. This decrease in both the gradient and thickness of the mixed layer is consistent with an upwelling event, although the wind speed data in Fig. 2 show no atypical features at this time. Upwelling events are common along the Southern California coast in early summer and usually are associated with sustained winds from the NW that push the surface waters to the west [2]. The breakdown in the sound speed gradient persists throughout most of the remainder of the experiment.

Over the second half of the experiment, the sound speed increased steadily at all depths, resulting in whole-water-column increases of 6-10 m/sec. This increase in sound speed at all depths is associated with the general increase in the average daily temperature over the second half of the experiment, seen in the upper panel of Fig. 4. The mixed layer thickened, extending to more than 15 m depth at experiment's end.

C. CDIP San Clemente Station Ocean Wave Heights

The CDIP San Clemente station is located at 33° 24.9′ N, 117° 37.8′ W, about 20 km to the NW of the ABM experiment site, in 10.2 m of water. The wave gauge array is composed of four

bottom pressure sensors located at the corners of a 6-m square [3].

1. Significant Wave Height

The significant wave height, i.e., the average height of the highest one-third of waves, calculated from the CDIP San Clemente station data is shown in the upper panel of Fig. 5. High wave events typically last 2-3 days with an inter-event period of 5-8 days. The increases in significant wave height starting on JD 124 (4 May), on JD 128 (8 May), and on JD 133 (13 May) appear to be associated with increases in sustained local wind speeds, shown again in the lower panel of Fig. 5. However, other notable wave events, e.g., the ones starting on JD 144 (24 May) and on JD 156 (5 June), do not correspond to any unusual feature in the wind speed data.

2. Peak Period Band

CDIP reports the wave energy spectra in the following 9 period bands; 4-6 sec, 6-8 sec, 8-10 sec, 10-12 sec, 12-14 sec, 14-16 sec, 16-18 sec, 18-22 sec, and 22+ sec. The band in which the wave energy is greatest is the "peak period band". The upper panel of Fig. 6 shows the peak period band time series. A definite association exists between wind speed and the peak period band. That is, increases in sustained winds in many cases are related to decreases in the surface wave peak period band, e.g., the events on JD 124-126 (4-6 May), JD 133 (13 May), and JD 161 (10 June). Conversely, times of low wind speed but fairly high significant wave heights appear associated with large peak periods.

3. Significant Angle

The lower plot in Fig. 6 shows the significant angle over time. The "significant angle" is calculated as the weighted average of the wave directions for each of 8 period bands (those bands listed in the previous paragraph minus the 22+ sec band), with the weighting equal to the band's percentage of the total wave energy [Coastal Data Information Program, private communication]. Fig. 6 shows that changes in the significant wave angle are strongly correlated with changes in

the peak period band; an increase in angle correlates with a decrease in peak period band and vice versa. The horizontal dotted line in the lower figure corresponds to the direction perpendicular to Red Beach [1]. The direction perpendicular to the beach off San Clemente is only slightly larger than the Red Beach value of 51°.

From the plots in Figs. 5 and 6, the following relationship appears to exist between the winds and the ocean surface wave data. Strong winds, blowing to the E-NE, give rise to short period (5-7 sec) waves that tend to propagate in the direction of the wind, i.e., E-NE. This direction corresponds to larger significant wave angles, 60-80°. During times of low wind, the wave peak period band in many cases increases to 15 sec. At these times, the waves tend to propagate in a more northerly direction (i.e., at smaller wave angles of 45-50°). Since the direction normal to Red Beach is 51°, then the direction of propagation of these longer period waves is probably dictated by the ocean bottom bathymetry. However, as Fig. 7 shows, deep water swell coming from the west and is prevented from reaching the Red Beach site by the islands of San Clemente, Santa Catalina, and San Nicolas, and that coming from the northwest is shadowed by the northern channel islands and the coast of California. Therefore, only the deep water swell coming from a southerly direction can reach the Red Beach site.

In summary, the events in the significant wave height plot appear to be of three types:

1. short-period, high-wind-speed, waves propagating to the E-NE in the direction of the local wind;
2. long-period, low-wind-speed, "distant" waves propagating perpendicular to the ocean bottom depth contours because of refraction and/or shadowing by S. California islands;
3. short-period events that don't appear to be correlated with increases in sustained local winds.

D. Measurements from the Deepest Oceanography Mooring

The deepest oceanography mooring was equipped with a bottom pressure sensor and two orthogonal, horizontal, electromagnetic current sensors. Its position was surveyed using a theodolite positioned on the shoreward side of the dirt road encircling the bluff on which the data acquisition van was located; the range to the mooring was 342 m. Since the distance from the theodolite position to the shoreline at mean tide was about 50 m, the offshore distance of the deepest mooring is about 300 m. The mooring recorded hourly data continuously throughout the experiment, starting at 19:00 GMT (12:00 PDT) on JD 123 (3 May).

1. "Significant Height" of the Ocean Bottom Pressure Fluctuations

Fig. 8 shows a comparison of the "significant bottom-pressure-fluctuation height" results from the deepest oceanography mooring with the significant wave heights from the CDIP San Clemente station. The two time series show the same features, suggesting that events seen in hourly averages of significant wave height are spatially homogeneous over the 20 km separation of the two moorings. However, the short-period wave events, particularly the 3-day event starting on JD 156 (5 June), are not nearly as prominent on the deep oceanography mooring results as they are in the CDIP results. This difference is due to the fact that CDIP makes a depth correction to their pressure data (collected in 10.2-m-deep water), to report ocean surface wave activity at the ocean surface, whereas the oceanography mooring results have not been depth-corrected. After accounting for the depth correction, the deep oceanography mooring results still appear to report smaller values than the CDIP array, by about 0.25 m. A small error in the assumed calibration value for one or both of these sensor installations probably is the source of the offset, although the possibility of a difference arising from their difference in location cannot be completely ruled out. The very-high-frequency component in the deep oceanography time series, causing its plot to appear darker, may have been reduced in the CDIP results by averaging the time series from the individual elements in their array.

2. Tide Heights

Fig. 9 shows a comparison of the tide height time series from the deepest oceanography mooring (upper panel) and from NOAA's tide station at La Jolla, Ca. (lower panel). Except for the difference in the reference value, the two time series appear identical. This fact is borne out by the coherence estimate between the two time series, plotted in Fig. 10. This estimate was calculated by incoherently averaging seven individual estimates -- equivalent to nearly 14 degrees of freedom after accounting for the percentage overlap and windowing of the input time series -- obtained with a 256-point FFT. The upper panel of Fig. 10 shows the coherence squared versus frequency and the lower panel shows the coherence phase in degrees. Vertical dotted lines are placed at the frequencies of 1 cycle/day and 2 cycles/day. At diurnal and semidiurnal frequencies, the two time series are perfectly correlated, as expected.

The coherence phase at the two frequencies can be used to determine the time delay in the tide heights between the two stations. Calculations of this type were performed between the three station pairs formed by the deep oceanography mooring, NOAA's La Jolla station, and NOAA's Santa Monica station. The following table contains the time delay results, along with the coherence phase estimate in parentheses.

Time Delay in Tide Heights from Coherence Estimates

Frequency (cycles/day)	Santa Monica/La Jolla (min)	Santa Monica/mooring (min)	mooring/La Jolla (min)
1	+12 (3.04°)	+20 (5.12°)	-8 (-2.09°)
2	+12 (6.05°)	+18 (9.07°)	-6 (-3.02°)

The west coast tide corrections listed in the back of the 1995 tide calendar for San Diego give the time delay between San Diego and Los Angeles as + 10 min, which compares favorably with the + 12-min estimate between La Jolla and Santa Monica given in the table. However, the time delay estimates involving the oceanography mooring data appear to be somewhat inaccurate,

probably because of a difference in the way the oceanography mooring and the NOAA data are processed to obtain hourly values.

3. Ocean Currents

The onshore (upper panel) and longshore (lower panel) components of current velocity from the horizontal electromagnetic current meters (EMCM) on the deepest oceanography mooring are presented in Fig. 11. Positive values represent flow in the shoreward and upcoast directions, respectively. The onshore component is significantly smaller than the longshore component due to the "boundary conditions" on the flow imposed by the coast. For the longshore component, large current velocities are directly related to the large wave events seen in the significant wave height data (re Fig. 7). The upcoast currents on JD 144-145 (24-25 May) and JD 166 (15 June), corresponding to the large-wave events at this same time, exceed 50 cm/sec (1 kt) in speed. In general, the largest currents are in the upcoast direction and are associated with large, long-period, "distant swell" events coming from the southerly direction. The somewhat smaller down-coast events are related to times of relatively high wind speed and short-period waves (re Fig. 5) coming from the west (re Fig. 6).

The fairly large upcoast current on JD 140 (20 May), associated with a long period wave event coming from a southerly direction, *may* be associated with the breakdown in the mixed layer and the sound speed gradient at this time seen in the lower panel of Fig. 4. That is, the breakdown may be due to mixing of deeper waters caused by long-period swell rather than upwelling from an Ekman boundary layer effect, as suggested earlier. However, the evidence from the data is too weak to support either arguement. The large downcoast current spike on JD 132 (12 May) may be associated with the high sustained winds on this day. However, this current event appears to precede, rather than follow, the wind, and so may have some other cause.

E. Highway 5 Traffic Counts and NOAA Tide Heights

The upper panel of Fig. 12 shows the hourly vehicle counts for both northbound (solid line) and southbound (dashed line) traffic along Highway 5, the major San Diego-to-Los Angeles freeway that passes within 0.5 km of the Red Beach experiment site. For comparison, the tides heights at NOAA's La Jolla station are replotted in the lower panel. The traffic data were collected by a California Department of Transportation (CalTrans) sensor just north of Oceanside Harbor exit. Since the Red Beach site is 0.5 km west of the Las Pulgas Road exit, the second exit north of Oceanside Harbor exit (the first exit north is a rest stop), then these vehicle count data are not a perfect count of the number of vehicles passing by the site. For example, traffic exiting at, or entering from, the rest stops on both sides of the freeway, the southbound traffic exiting at Las Pulgas Road, and the northbound traffic entering at Las Pulgas Road are not accurately accounted for. However, these errors have a minimal impact on the quality of the data. Also, although the data do not contain information on vehicle type, historical studies have shown that 89 % of the traffic are automobiles and 11 % are trucks, with the truck types categorized as: 38 % are 2 axle, 7.5 % are 3 axle, 6.5 % are 4 axle, and 48 % are 5+ axle vehicles [R. Triplett, CalTrans, private communication].

Close examination of the traffic count time series shows that the vehicle counts in both directions reach a minimum of a few hundred vehicles per hour in the early morning hours between 2-4 am local time. The morning rush-hour traffic is represented as a spike in the northbound direction as commuters head to jobs in the Los Angeles area. A corresponding spike in the southbound traffic time series later in the day indicates the evening commute. A weekly component of variation is present, with a large number of vehicles heading southward on Fridays and Saturdays and a large northbound spike on Sundays.

Clearly, though, the dominant component of variability in both the traffic count and the tide height time series is diurnal. To illustrate this correspondence, the coherence squared estimate

between the tide heights and the northbound traffic is shown in Fig. 13. A large peak with amplitude of 0.9 occurs at 1 cycle/day, indicating that 90 % of the variability at 1 cycle/day in one of the time series can be predicted by the variability at this frequency in the other time series. Two additional spikes with coherence squared values above 0.5 occur at about 7.25 cycles/day and at 9.5 cycles/day.

F. Environmental Data from Source Tows

On JD 161 (10 June), nearly 3.5 hours of underwater acoustic source tows were conducted. Fig. 14 shows the track of the source tow ship in relation to the positions of the two bottom hydrophone arrays, the shoreline, and the data acquisition van. The border of this plot is represented by the large dark rectangle in Fig. 1. The ship track starts to the southeast at 18:13:03 GMT, and ends to the north of the arrays at 20:25:32 GMT. Attached to the source tow cable was a General Oceanics inclinometer that internally recorded the depth, temperature, inclination, and direction of inclination. The instrument was programmed to record a sample once every 10 sec starting at 17:33:06 GMT.

During the source tow and afterwards, a fishfinder made by Eagle (model Vita 2) was used to acoustically measure the water depth. These measurements were recorded by hand into the scientific log approximately every 10 min.

1. Inclinometer Depth and Temperature

Fig. 15 shows the inclinometer depth (upper panel) and temperature (lower panel) time series over the 3.5-hour recording period. For the first 9 min and the last half-hour, the inclinometer was not deployed at depth, so that useful data were collected only during the period 17:42 - 20:34 GMT. While deployed, the sensor depth varied by one quantization interval of 0.5 m about 5 m, and the water temperature varied between 18.0° C and 18.5° C. The temperature after 90 min or so into the time series has a higher frequency component of variability than over the first

90 min. This change occurs about the same time that the ship turned towards the coast -- at 19:02 GMT -- after finishing the first track from the southeast to the northwest; re Fig. 14. The increase in variability after the turn may be indicative of a larger spatial and/or temporal variability in water temperature at 5 m as the surf zone is approached. (Variations due to small changes in inclinometer depth resulting from an increase in ship maneuvering also may play a role). The average water temperature over the 17:42 - 20:34 time period was used to estimate the 5-m sound speed value on JD 161 in the lower panel plot of Fig. 4.

2. Fishfinder-Derived Water Depth

The Eagle fishfinder uses the two-way travel-time of a high-frequency acoustic ping along with an assumed sound speed to measure water depth. Fishfinders and echosounders typically use an unrealistically small sound speed to calculate depth to provide a margin of safety in preventing ships running aground. For example, the Eagle fishfinder uses a value of 4550 ft/sec, equal to 1387 m/sec, so that its depth output must be corrected. In addition, the distance of the fishfinder below the ocean surface and tidal variations must be taken into account. Fig. 16 shows the time series of the corrected water depth obtained from the fishfinder readout recorded by hand in the scientific log. The upper plot is for the same time period and has the same horizontal scale as the inclinometer plots in Fig. 15. The nearly-constant water depth of 20-21 m along the first track from the southeast towards the arrays is followed by a "hill", with a 10-m-deep peak, representing the tracks towards, along, and then away from the surf zone (re Fig. 14).

The towed acoustic source system failed prematurely, at the northern end of the northbound track shown in Fig. 14. Therefore, the source event proceeded by having the Harbor Chief, the source tow ship, run a prescribed set of tracks at constant speed, with the ship-radiated noise replacing the towed source signals. The lower plot in Fig. 16 shows the water depth time series over the full source event on JD 161. The time period covered by the curve in the upper plot is bracketed by the two vertical dotted lines. The large increase in water depth about 270 min into

the lower time series is the result of a run out to deeper waters, used to "calibrate" the propagation of distant shipping noise from the W/NW.

II. SPATIAL DISTRIBUTION of the DATA

A. CTD Sound Velocity Profiles

A total of 15 CTD casts were taken over the 8-week period of the experiment. A plan view of the locations of these casts is given in Fig. 17. This plot is on the same scale as in Fig. 14, and its border is plotted in Fig. 1. In general, these cast locations are close to the locations of the moored sonobuoys and the bottom hydrophone arrays deployed during the experiment. On three days, JD 140 (20 May), JD 145 (25 May), and JD 165 (14 June), consecutive CTD profiles were taken along tracks nearly perpendicular to the shoreline. These tracks are indicated by dashed lines in the figure. Plots of the CTD-derived sound speed profiles as a function of distance along these tracks are shown in Figs. 18, 19, and 20, for each of the three days. A slight decrease of 1-2 m/sec in the near-surface sound speed with distance along the track is evident in these plots. However, the main feature is the deepening of the mixed surface layer with distance, particularly on JD 165. On JD 165, the two profiles nearest to shore have mixed layers that are half as deep as those in deeper water, providing a range dependence to the sound speed structure in addition to that provided by the water depth changes. For JD 140 and 145, the sound speed's range dependence is much weaker.

B. Environmental Data from Source Tows

1. Inclinometer Temperature

Fig. 21 shows a contour plot of the inclinometer-measured water temperature at 5 m depth covering a 2.5 km by 2.5 km area. The contour lines occur in 0.1° C increments. Superimposed on the figure is the source tow track. Except for possible warm spots 600 m to the east and 1000 m to the north of the arrays, the water temperature appears to be spatially homogeneous over the

area.

2. Fishfinder-Derived Water Depth

Fig. 22 is a second contour plot, covering the same area as in Fig. 21, this time showing the water depth obtained from the fishfinder soundings during the source tow. The contours are spaced at 1 m depth increments. Apparently, the arrays were deployed on the western side of a region with a slightly greater slope, about 0.5°, than the immediately-surrounding area. The northeastern side of the plot shows the bottom contours being approximately parallel to the coast-line, with slopes of 0.1 - 0.2°. These data will be merged with near-shore water depth surveys of the Red Beach area conducted by Navy SEALs [1] and used as geoacoustic model inputs to range-dependent seismoacoustic propagation codes.

CONCLUSIONS and RECOMMENDATIONS

Several types of environmental measurements were obtained to support the seismoacoustic data collected during the Adaptive Beach Monitoring pilot experiment. By simply plotting the various types of environmental measurements on the same time scale, associations between the data can be drawn. For example, early-summer warming can be seen in both the air and water temperatures, which in turn affects the propagation of sound in these two media. Fairly clear relationships exist between wind speed and direction, ocean surface wave activity (amplitudes, directions of propagation, and predominant periods), and ocean currents. In many cases, the most dominant feature of the time series is the diurnal component of variability. This observation can be quantified by estimating coherences between time series; e.g., 90 % of the variability at diur-nal periods in hourly traffic counts along Highway 5 is linearly related to the diurnal fluctuations in tide heights.

The predominance of the diurnal component of variability in many of the environmental data sets should be taken into account in designing seismoacoustic data sampling strategies in

future experiments. That is, those sensor systems that do not record data continuously ought to record blocks of data at time periods that permit an adequate sampling of diurnal fluctuations. Actually, this recommendation should be followed in collecting the environmental measurements themselves -- in particular, ocean water temperature. Shortcomings in water temperature measurements can be eliminated in the future by deploying one or more self-recording thermistor strings, preferably co-located with the seismoacoustic sensors. With an adequately high data sampling rate, these data also can be used to examine internal wave activity and its potential effect on higher frequency sound propagation. Also, spatial coverage of ocean temperature measurements should be improved. One way is to perform a set of CTD profiles along a small set of predetermined tracks during each sea trip. Another improvement would be to deploy the inclinometer for a longer period of time, along tracks with a greater spatial coverage. This recommendation will be easily satisfied since much more extensive underwater acoustic source tows already are planned for the next experiment. Finally, satellite sea surface temperature maps can be obtained to provide insight into the regional oceanographic changes that affect the study site.

ACKNOWLEDGEMENTS

Thanks are due to the Range Scheduling Office, Marine Corps Base, Camp Pendleton for giving permission to conduct this pilot experiment on Red Beach. Lieutenant Colonel Settle, Terry Finch, and Warrant Officer Cooper provided the support required to get the operations underway. Without the support of the Commander, Amphibious Group Three, this experiment would not have occurred. A special acknowledgement is due to Commander Craig Madsen of Amphibious Group Three, whose recognition of the potential advantages to Amphibious Warfare of the Adaptive Beach Monitoring system and his support for the experiment were instrumental in allowing MPL to stage this experiment. Special thanks also are extended to Ms. Ann Rosenberry, Code 232, Southwest Division, Naval Facilities Engineering Command, for her valuable assistance in ensuring compliance with State and federal environmental regulations. Her

assistance was invaluable to the success of this pilot experiment. In addition, the cooperation of the Commander, U. S. Third Fleet is appreciated.

NRaD code 541 generously loaned us the CTD to make the sound speed measurements. The 10-m weather station was installed and operated by the Center for Coastal Studies, Scripps Institution of Oceanography. Dean Carlson of the R/V Fisherette and Robert Mitchell ("Mitch") and Mike Kyle who crewed the Harbor Chief provided valuable support in the sea-going operations. Finally, Robert J. Triplett, the Traffic Census Coordinator at CalTrans, provided us with the Highway 5 vehicle count data.

Dave Ensberg of MPL created the two contour plots shown in Figs. 20 and 21.

The Adaptive Beach Monitoring program is sponsored by the Office of Naval Research, Code 32. The principal investigators are W. A. Kuperman, W. S. Hodgkiss, L. M. Dorman, W. A. Gaines, K. Melville, G. Deane, and G. L. D'Spain.

APPENDIX

List of Environmental and Ancillary Data from the ABM Pilot Experiment

Data Type	Sensor System
Basic Weather Data i. wind speed and direction ii. air temperature iii. relative humidity iv. barometric pressure	A. 10-m weather station from CCS B. 2 miniature ARL/PSU met stations
Water Properties	A. 15 CTD casts B. inclinometer temperature sensor C. CalCOFI report for Apr, 1995 cruise [4]
Ocean Surface Wave Activity	A. 2 bottom pressure sensors at moorings 20 m and 300 m offshore B. CDIP stations at San Clemente and Oceanside [3] C. 2 videocameras
Ocean Currents	A. 2 EM current meters at deepest mooring
Water Depth	A. shipboard fishfinder during source tows B. Navy SEAL survey of Red Beach [1]
Tide Heights	A. NOAA stations at La Jolla and Santa Monica, CA B. bottom pressure sensors at two offshore moorings
Hwy 5 Traffic Activity	A. CalTrans vehicle counter
Train Activity	A. Amtrak train schedule
Ocean Bottom Geoacoustic Properties	A. Report on San Onofre bottom cores [5] B. J. Northrop, J. Acoust. Soc. Am. paper [6]
Earthquake Activity	A. Southern California Earthquake Center Reports [7]

REFERENCES

[1] Red Beach survey, SEAL team 5, 25 July, 1994.

[2] B. Hickey, "The California Current system - hypotheses and facts", in *Progress in Oceanography*, 1979.

[3] The Coastal Data Information Program, Scripps Institution of Oceanography, World Wide Web home page at the Uniform Resource Locator (URL) http://splash.ucsd.edu/homepage.html, data retrieved in Summer, 1995.

[4] The Marine Life Research Group, Scripps Institution of Oceanography, World Wide Web home page at the URL http://www-mlrg.ucsd.edu/mlrghome.html, data retrieved in Fall, 1995.

[5] San Onofre Sediment Dynamics Group, "Sediment Dynamics of the Area off San Onofre, California", R. Kolpack, ed. and project manager, submitted to Environmental Research, Southern California Edison Company, P. O. Box 800, Rosemead, CA, Oct., 1990.

[6] J. Northrop, "Low-frequency sound propagation off Mission Beach, California", J. Acoust. Soc. Am., 67(5), pp. 1598-1602, 1980.

[7] The Southern California Earthquake Center, California Institute of Technology, World Wide Web home page at the URL http://scec.gps.caltech.edu, data retrieved in Summer, 1995.

Figure Captions

Figure 1. The part of the Camp Pendleton chart where the Adaptive Beach Monitoring Pilot Experiment was conducted. The data acquisition van was located on a 3-m tall bluff at the northern end of Red Beach (indicated by a circled "RB" in the figure. The coastline runs northwest-southeast in the upper right corner of the figure (the normal to Red Beach is 51° [1]). Highway 5, a major freeway between San Diego and Los Angeles, runs subparallel to the coastline to the northeast. The circled "LHA" indicates the location of a helicopter landing pad. At the southeastern end of the figure, the major LCAC offshore transit lane runs perpendicular to shore. Also, the heavy diagonal line in the southwest corner shows the along-shore LCAC transiting lane. The dotted line cutting a diagonal across the figure signifies the boundaries of the AAV training area. The grid squares on the chart are each 1000 m on each side. The large dark rectangle marks the border of the plan view plots shown in Fig. 14 and 17.

Figure 2. Wind speed and direction the wind is blowing *TO*, from the 10-m weather station.

Figure 3. Barometric pressure and relative humidity, from the 10-m weather station.

Figure 4. Air temperature, from the 10-m weather station, and sound speeds at 1 ("1"), 5 ("5"), 10 ("A"), 15 ("E"), and 20 ("2") m depth, from the CTD casts and the inclinometer temperature measurements at 5 m depth.

Figure 5. Ocean surface wave significant wave height, from the Coastal Data Information Program bottom pressure sensor array at San Clemente, and the wind speed amplitude, from the 10-m weather station.

Figure 6. Ocean surface wave peak period band and significant wave angle specifying the predominant direction the waves are traveling *TO*, both from the CDIP bottom pressure sensor array at San Clemente. The horizontal dashed line in the lower plot indicates the direction normal to Red Beach.

Figure 7. Map showing the predictions of the Southern California Swell Model for 23 Aug, 1995, from the Coastal Data Information Program World Wide Web site.

Figure 8. "Significant bottom-pressure-fluctuation height", from the deepest oceanography mooring, and the ocean surface wave significant wave height, from the CDIP bottom pressure sensor array off San Clemente.

Figure 9. Tide heights, from the deepest oceanography mooring and from NOAA's La Jolla station, respectively.

Figure 10. Coherence squared and phase estimate between the hourly tide heights from the deepest oceanography mooring and NOAA's La Jolla station. Vertical dashed lines mark the frequencies of 1 and 2 cycles/day.

Figure 11. Onshore and longshore components of ocean current velocity, from the two horizontal electromagnetic current meters (EMCM) at the deepest oceanography mooring. Positive values indicate onshore and upcoast flows, respectively.

Figure 12. North-bound (solid curve) and south-bound (dashed curve) traffic counts on Highway 5, from the CalTrans sensor just north of the Oceanside Harbor exit, and tide heights, from NOAA's La Jolla station.

Figure 13. Coherence squared estimate between the hourly tide heights and north-bound traffic counts.

Figure 14. Plan view of the source tow tracks on JD 161. The positions of the two bottom hydrophone arrays are indicated by straight lines with diamonds at each end. The location of the data acquisition van on Red Beach is shown as a square in the northwest corner, next to the coastline. The ship started to the southeast and finished to the north of the arrays.

Figure 15. Time series over 3.5-hour period of the depth (upper plot) and temperature (lower plot) recorded by the inclinometer attached to the source tow cable.

Figure 16. Time series of the fishfinder-derived water depths along the source tow track and afterwards on JD 161. The upper plot covers the period when the towed source was deployed and has the same horizontal time scale as in Fig. 15. The lower plot shows the water depths over the full source event on JD 161, where the time period covered by the upper plot's curve is bracketed by the two vertical dotted lines.

Figure 17. Plan view of the experiment site showing the locations of the 15 CTD casts taken during the experiment. The size of the area plotted is approximately 3.3 km by 2.8 km and is the same as in Fig. 14. On three days in the experiment, consecutive CTD casts were taken along tracks approximately perpendicular to the beach. These CTD locations are connected by dashed lines; those taken on JD 140 (20 May) are along the SE-most track, those on JD 165 (14 June) are on the NW-most track, and those on JD 145 (25 May) are along the track in the middle. The location of the coastline is indicated by the solid diagonal line in the upper right corner of the plot, and the data acquisition van next to the beach is plotted as a square. The hourglass symbol near the coastline marks the position of the deepest oceanography mooring.

Figure 18. Plots of the sound speed profiles versus depth and distance along the track, from the set of three CTDs taken on JD 140 (20 May). This track is the SE-most one in Fig. 17. The horizontal offset of the first (shallowest) cast is the distance of the cast from the shoreline; the other two casts are offset according to their distance along the track. The CTD profiles are centered on the vertical dashed lines specifying a sound speed of 1505 m/sec. The horizontal scale of the sound speed profiles, from 1495 m/sec to 1515 m/sec with tick marks at 5 m/sec increments, are given by the horizontal lines at the top of each profile.

Figure 19. Plots of the sound speed profiles versus depth and distance along the track, from the set of three CTDs taken on JD 145 (25 May) (the middle track in Fig. 17). The other

features of this plot are identical to those of Fig. 18.

Figure 20. Plots of the sound speed profiles versus depth and distance along the track, from the set of four CTDs taken on JD 165 (14 June) (the NW-most track in Fig. 17). The other features of this plot are identical to those of Figs. 18 and 19, except that the horizontal sound speed axis for the second profile is below, rather than at the top, of the profile.

Figure 21. Contour plot of the inclinometer-derived water temperature at 5 m depth covering a 2.5 km by 2.5 km area, from 33° 16.00′ to 33° 17.3499′ N and 117° 28.3854′ to 117° 30.00′ W. The contour lines occur in 0.1° C increments. These data were taken during the underwater acoustic source tow on JD 161 (10 June), while the source was at depth from 17:42 to 20:34 GMT. Superimposed on the figure is the source tow track.

Figure 22. Contour plot of the water depths in 1 m depth increments determined by the shipboard fishfinder during the source tows on JD 161 (10 June). The area of the plot is the same as in Fig. 21 and the source tow track is again superimposed on the figure.

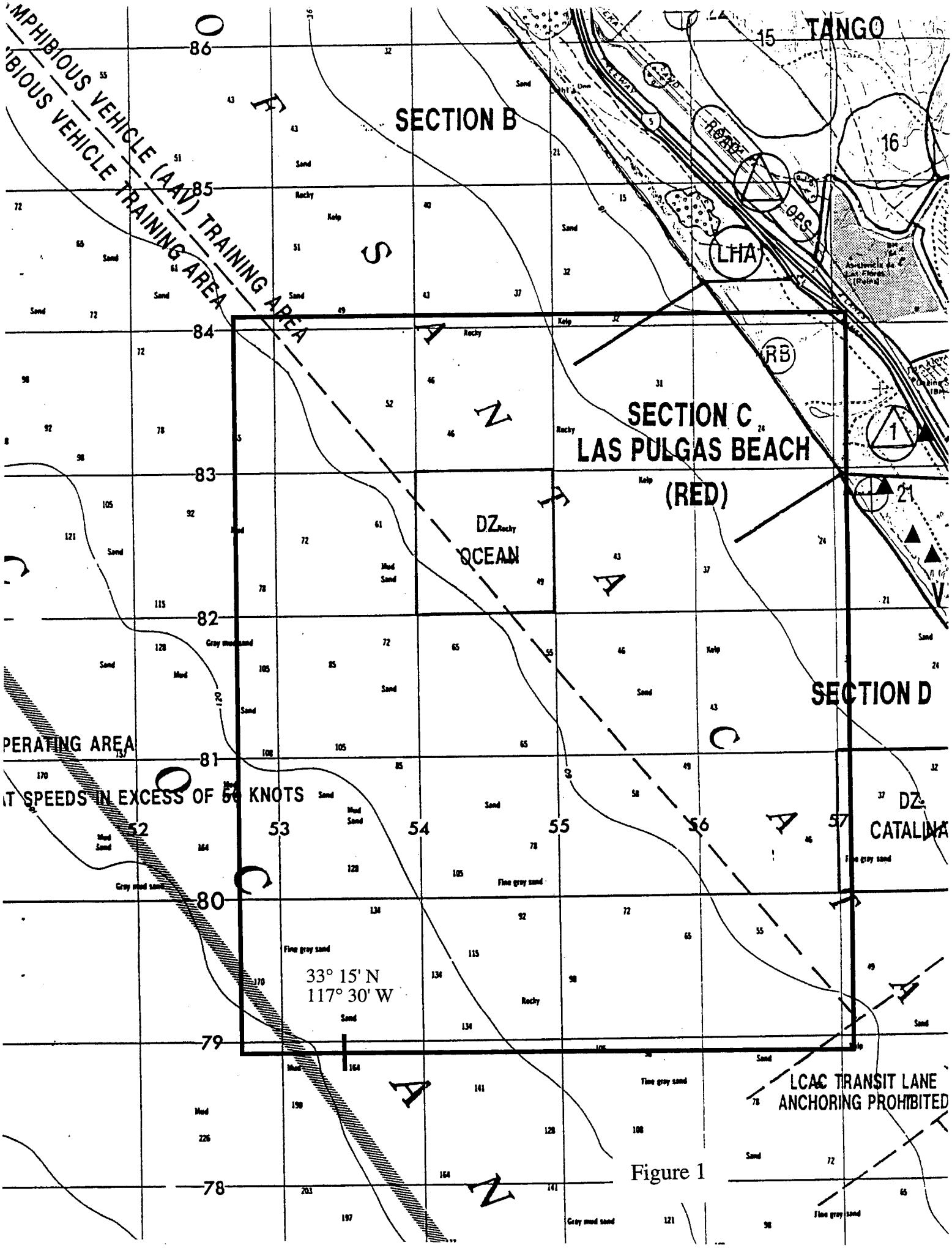
MPHIBIOUS VEHICLE (AAV) TRAINING AREA
IBIOUS VEHICLE TRAINING AREA
SECTION B
SECTION C
LAS PULGAS BEACH
(RED)
SECTION D
DZ Rocky
OCEAN
LHA
RB
TANGO
15
16
21
1
86
85
84
83
82
81
80
79
78
52
53
54
55
56
57
PERATING AREA
T SPEEDS IN EXCESS OF 60 KNOTS
33° 15' N
117° 30' W
DZ
CATALINA
LCAC TRANSIT LANE
ANCHORING PROHIBITED

Figure 1

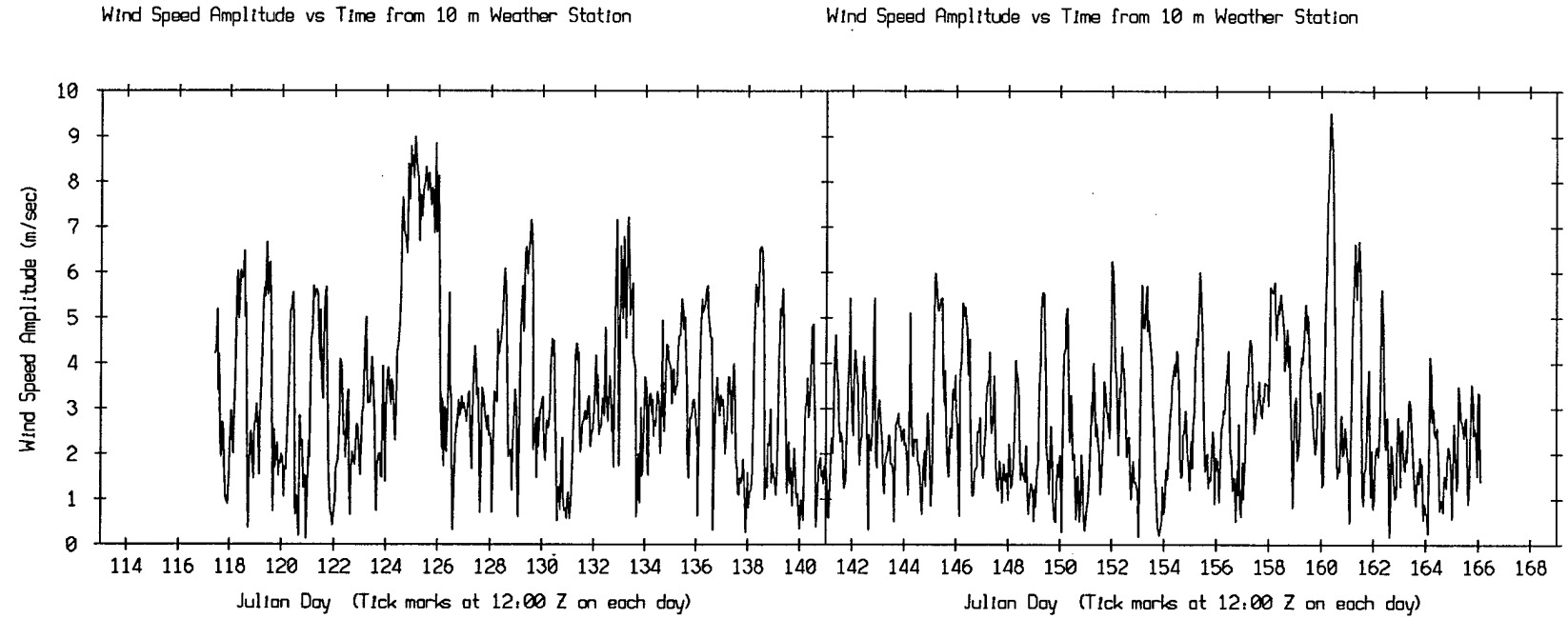
Wind Speed Amplitude vs Time from 10 m Weather Station
Wind Speed Amplitude (m/sec)
0
1
2
3
4
5
6
7
8
9
10
114 116 118 120 122 124 126 128 130 132 134 136 138 140
Julian Day (Tick marks at 12:00 Z on each day)
Wind Speed Amplitude vs Time from 10 m Weather Station
142 144 146 148 150 152 154 156 158 160 162 164 166 168
Julian Day (Tick marks at 12:00 Z on each day)

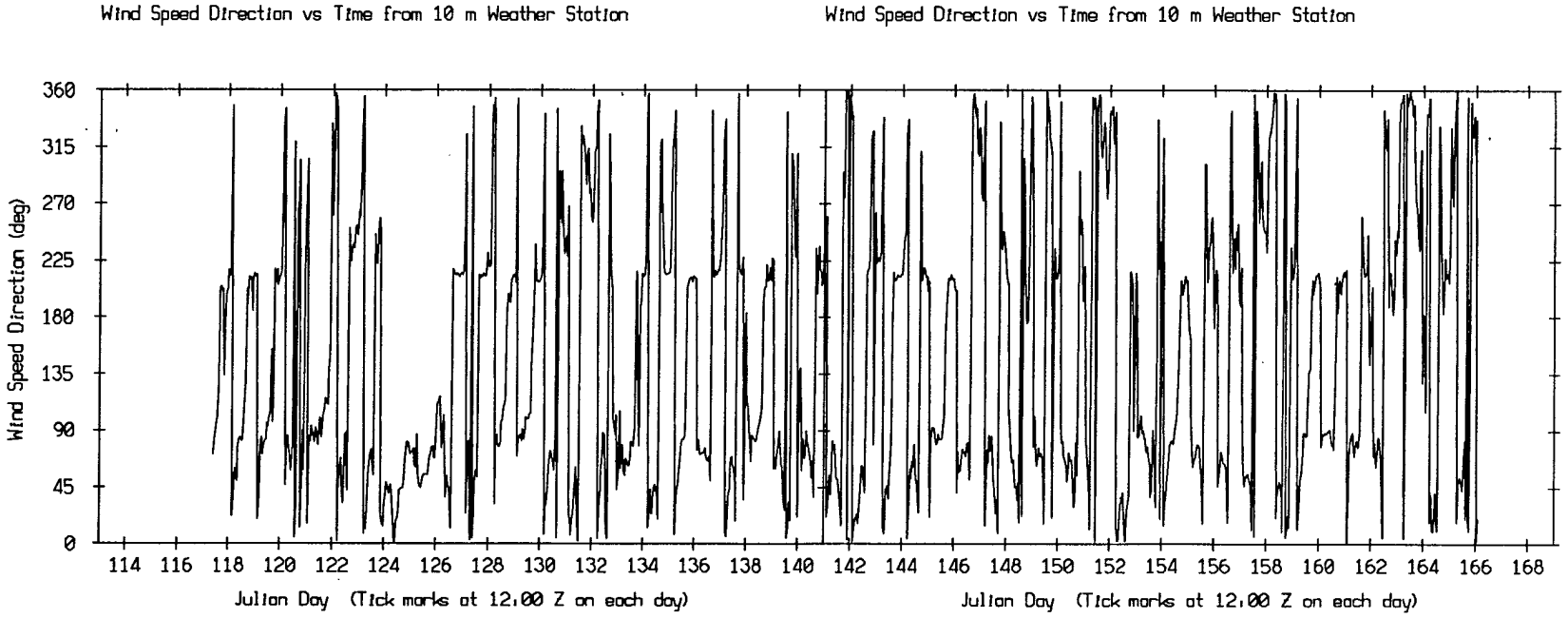
Wind Speed Direction vs Time from 10 m Weather Station
Wind Speed Direction (deg)
0
45
90
135
180
225
270
315
360
114 116 118 120 122 124 126 128 130 132 134 136 138 140
Julian Day (Tick marks at 12:00 Z on each day)
Wind Speed Direction vs Time from 10 m Weather Station
142 144 146 148 150 152 154 156 158 160 162 164 166 168
Julian Day (Tick marks at 12:00 Z on each day)

Figure 2

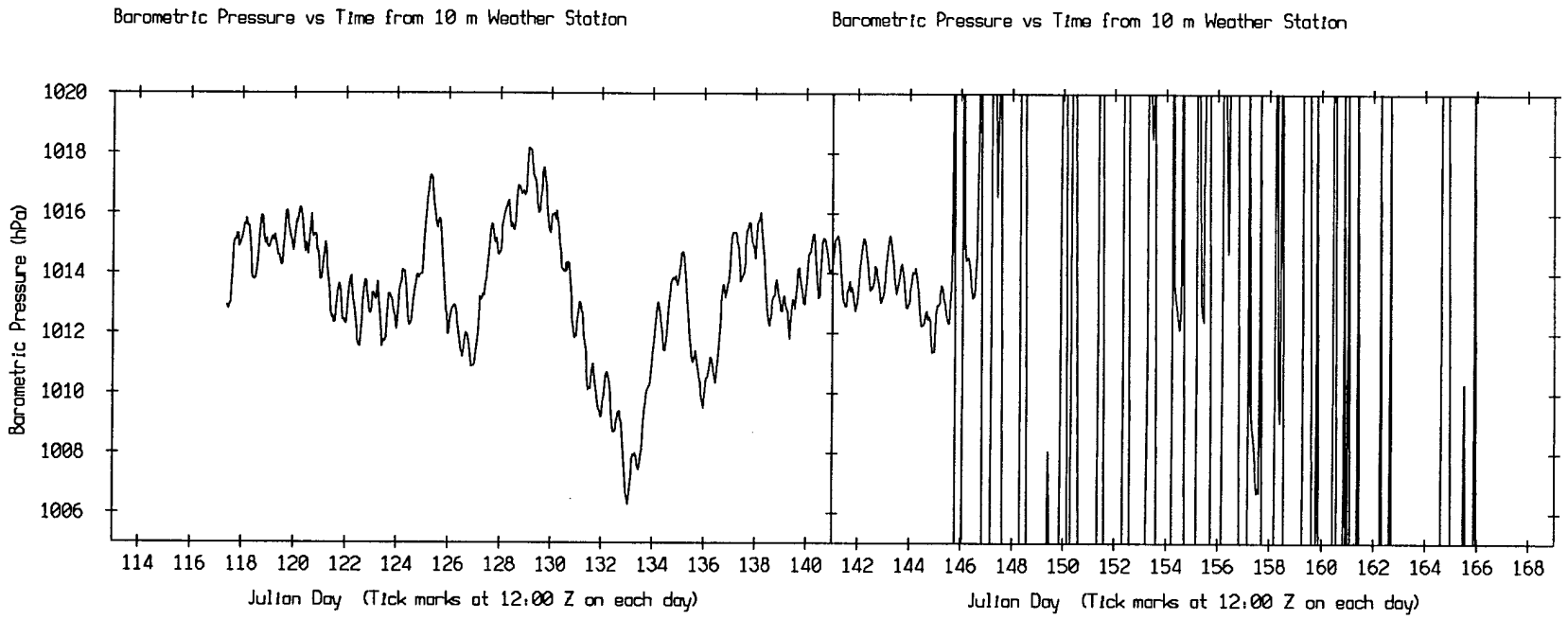
Barometric Pressure vs Time from 10 m Weather Station
Barometric Pressure vs Time from 10 m Weather Station
Barometric Pressure (hPa)
1020
1018
1016
1014
1012
1010
1008
1006
114 116 118 120 122 124 126 128 130 132 134 136 138 140 142 144 146 148 150 152 154 156 158 160 162 164 166 168
Julian Day (Tick marks at 12:00 Z on each day)
Julian Day (Tick marks at 12:00 Z on each day)

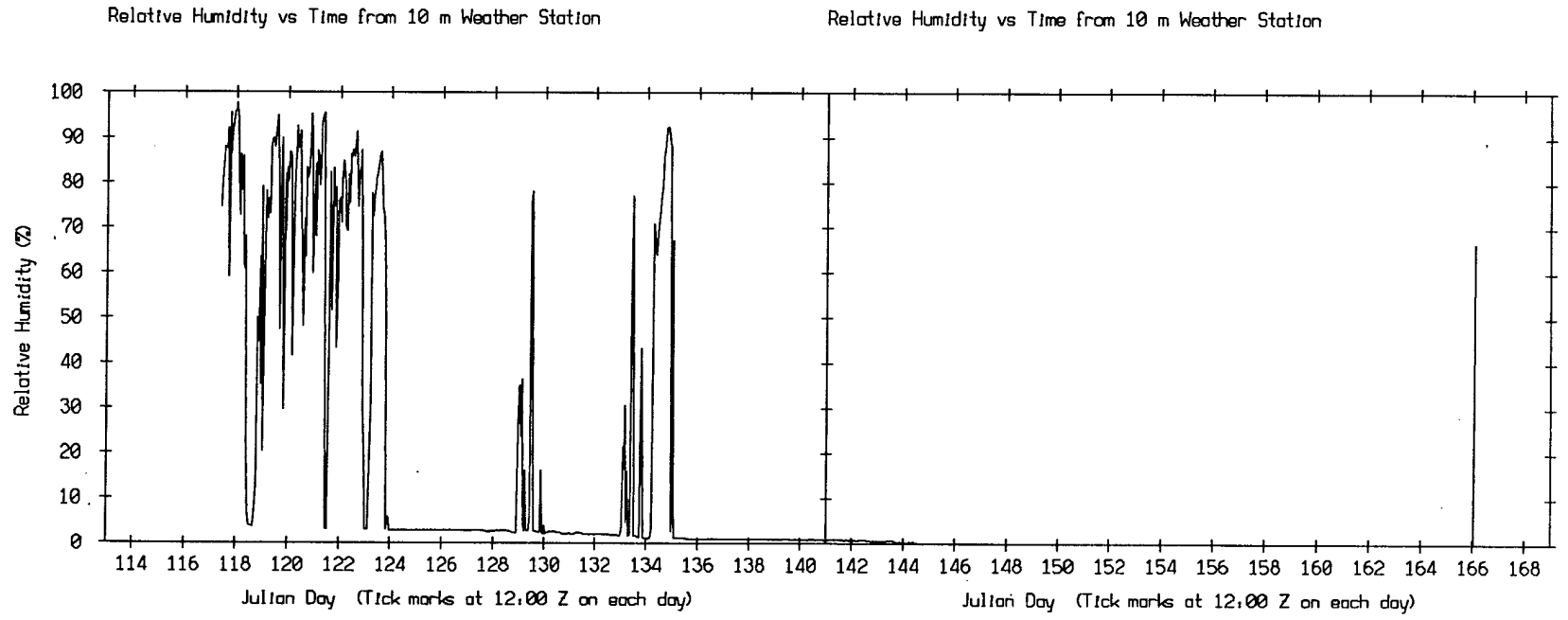
Relative Humidity vs Time from 10 m Weather Station
Relative Humidity vs Time from 10 m Weather Station
Relative Humidity (%)
100
90
80
70
60
50
40
30
20
10
0
114 116 118 120 122 124 126 128 130 132 134 136 138 140 142 144 146 148 150 152 154 156 158 160 162 164 166 168
Julian Day (Tick marks at 12:00 Z on each day)
Julian Day (Tick marks at 12:00 Z on each day)

Figure 3

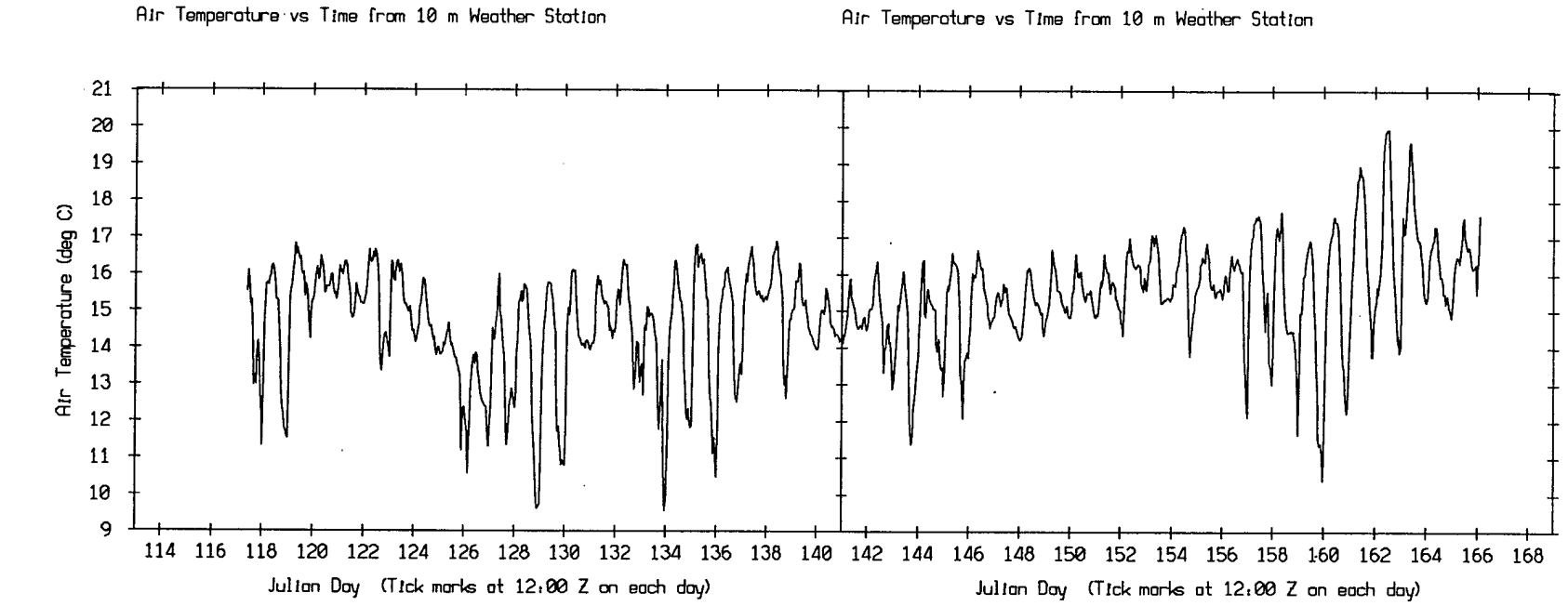
Air Temperature vs Time from 10 m Weather Station
Air Temperature vs Time from 10 m Weather Station
Air Temperature (deg C)
21
20
19
18
17
16
15
14
13
12
11
10
9
114 116 118 120 122 124 126 128 130 132 134 136 138 140
142 144 146 148 150 152 154 156 158 160 162 164 166 168
Julian Day (Tick marks at 12:00 Z on each day)
Julian Day (Tick marks at 12:00 Z on each day)

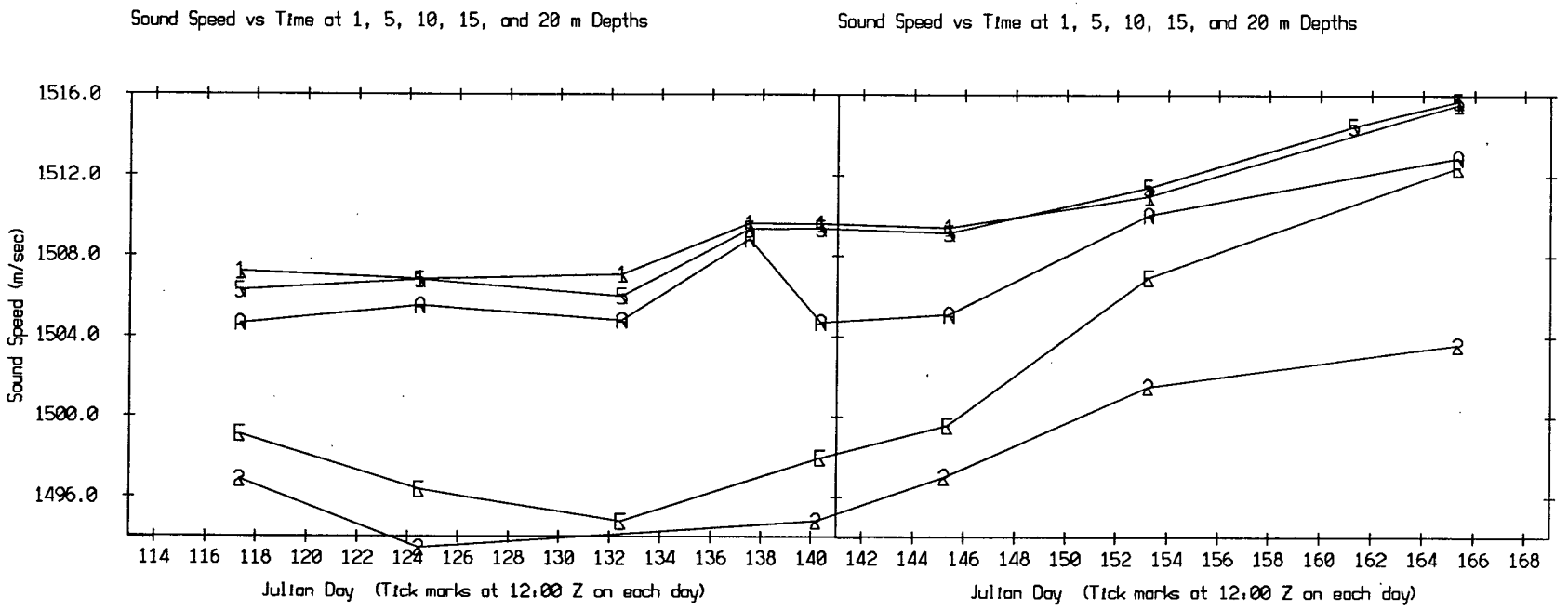
Sound Speed vs Time at 1, 5, 10, 15, and 20 m Depths
Sound Speed vs Time at 1, 5, 10, 15, and 20 m Depths
Sound Speed (m/sec)
1516.0
1512.0
1508.0
1504.0
1500.0
1496.0
114 116 118 120 122 124 126 128 130 132 134 136 138 140
142 144 146 148 150 152 154 156 158 160 162 164 166 168
Julian Day (Tick marks at 12:00 Z on each day)
Julian Day (Tick marks at 12:00 Z on each day)

Figure 4

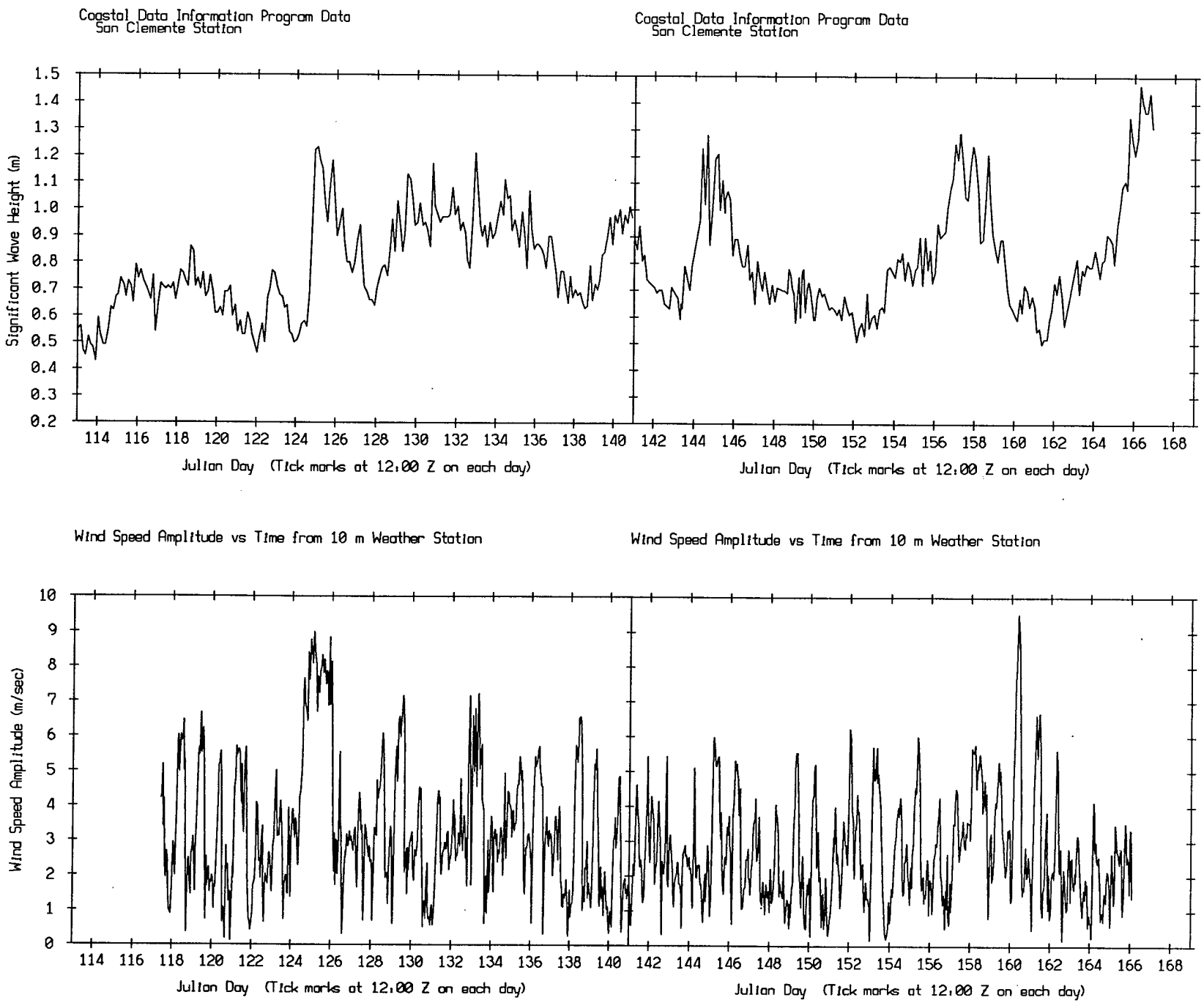
Coastal Data Information Program Data
San Clemente Station
Significant Wave Height (m)
1.5
1.4
1.3
1.2
1.1
1.0
0.9
0.8
0.7
0.6
0.5
0.4
0.3
0.2
114 116 118 120 122 124 126 128 130 132 134 136 138 140
Julian Day (Tick marks at 12:00 Z on each day)
Coastal Data Information Program Data
San Clemente Station
142 144 146 148 150 152 154 156 158 160 162 164 166 168
Julian Day (Tick marks at 12:00 Z on each day)
Wind Speed Amplitude vs Time from 10 m Weather Station
Wind Speed Amplitude (m/sec)
10
9
8
7
6
5
4
3
2
1
0
114 116 118 120 122 124 126 128 130 132 134 136 138 140
Julian Day (Tick marks at 12:00 Z on each day)
Wind Speed Amplitude vs Time from 10 m Weather Station
142 144 146 148 150 152 154 156 158 160 162 164 166 168
Julian Day (Tick marks at 12:00 Z on each day)

Figure 5

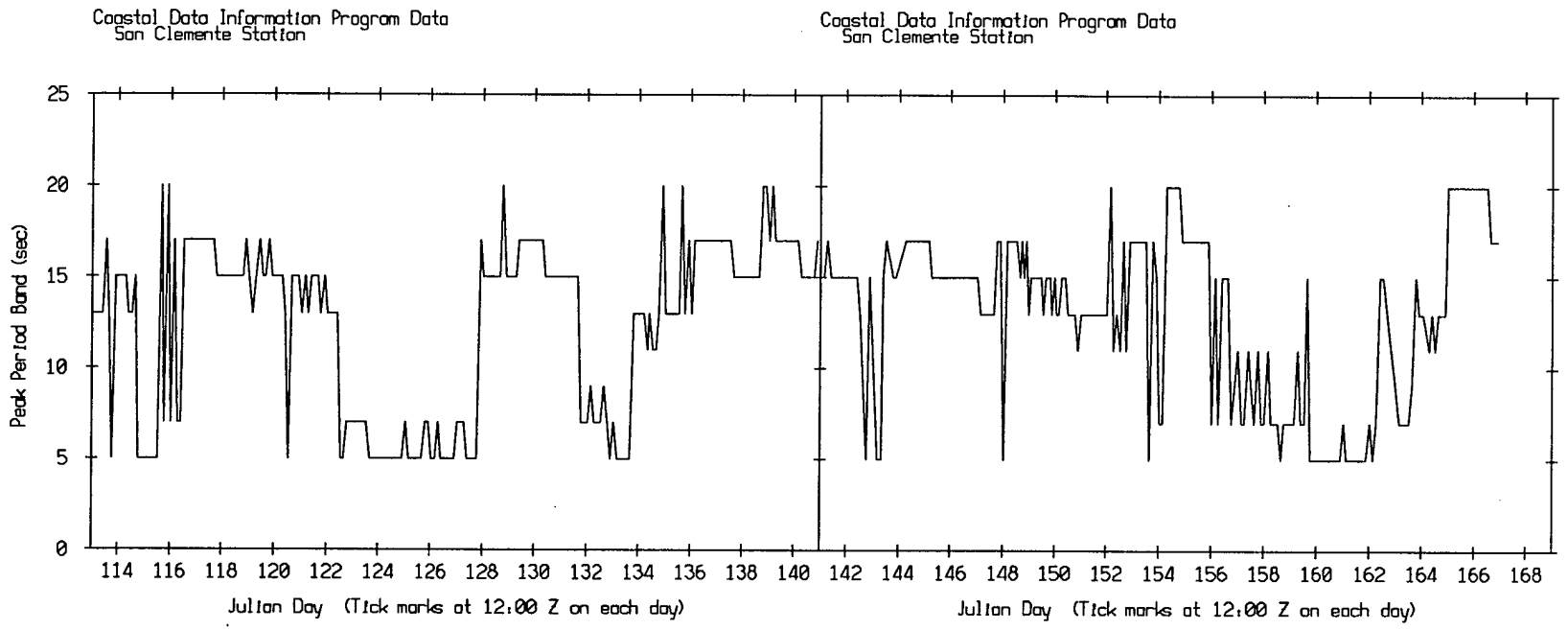
Coastal Data Information Program Data
San Clemente Station
Peak Period Band (sec)
25
20
15
10
5
0
114 116 118 120 122 124 126 128 130 132 134 136 138 140
Julian Day (Tick marks at 12:00 Z on each day)
Coastal Data Information Program Data
San Clemente Station
142 144 146 148 150 152 154 156 158 160 162 164 166 168
Julian Day (Tick marks at 12:00 Z on each day)

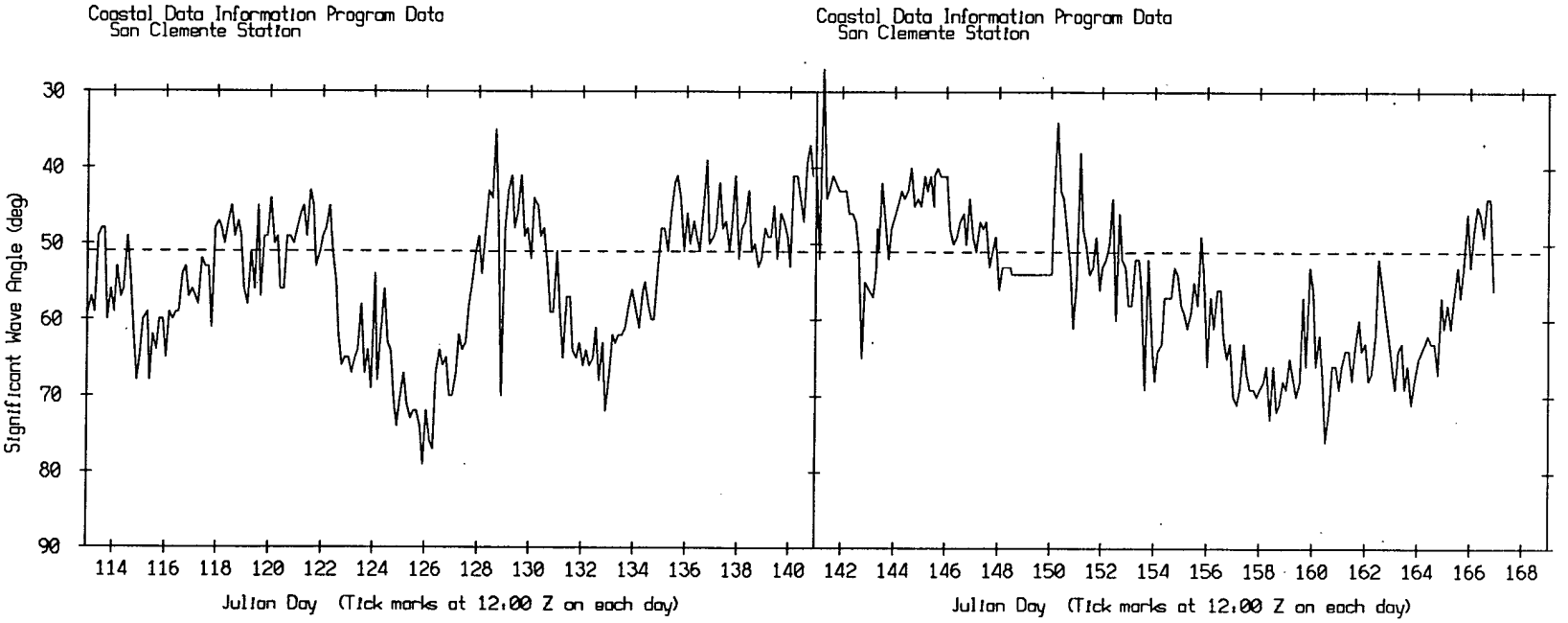
Coastal Data Information Program Data
San Clemente Station
Significant Wave Angle (deg)
30
40
50
60
70
80
90
114 116 118 120 122 124 126 128 130 132 134 136 138 140
Julian Day (Tick marks at 12:00 Z on each day)
Coastal Data Information Program Data
San Clemente Station
142 144 146 148 150 152 154 156 158 160 162 164 166 168
Julian Day (Tick marks at 12:00 Z on each day)

Figure 6

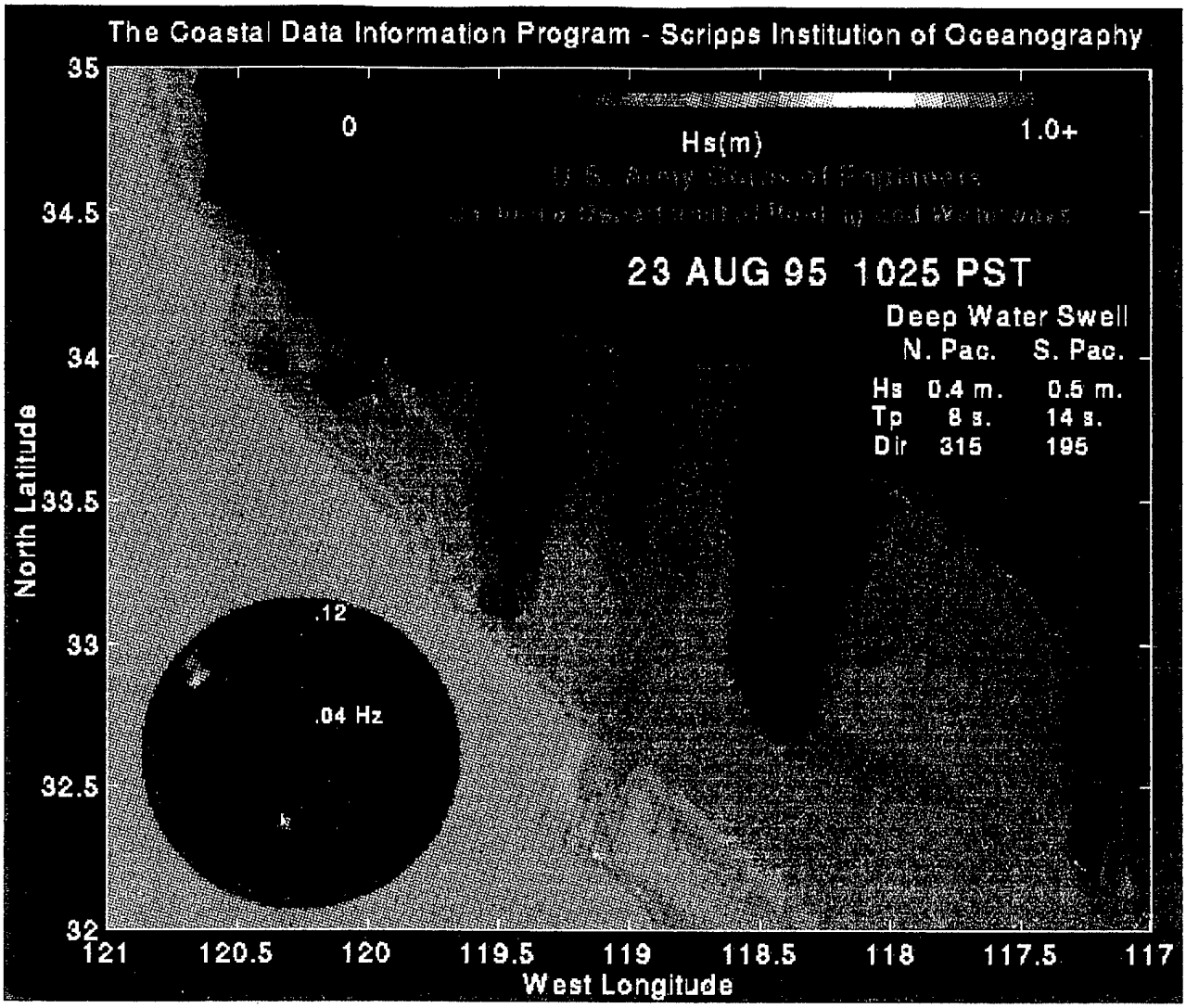
The Coastal Data Information Program - Scripps Institution of Oceanography
0
Hs(m)
1.0+
23 AUG 95 1025 PST
Deep Water Swell
N. Pac. S. Pac.
Hs 0.4 m. 0.5 m.
Tp 8 s. 14 s.
Dir 315 195
.12
.04 Hz
35
34.5
34
33.5
33
32.5
32
North Latitude
121
120.5
120
119.5
119
118.5
118
117.5
117
West Longitude

Figure 7

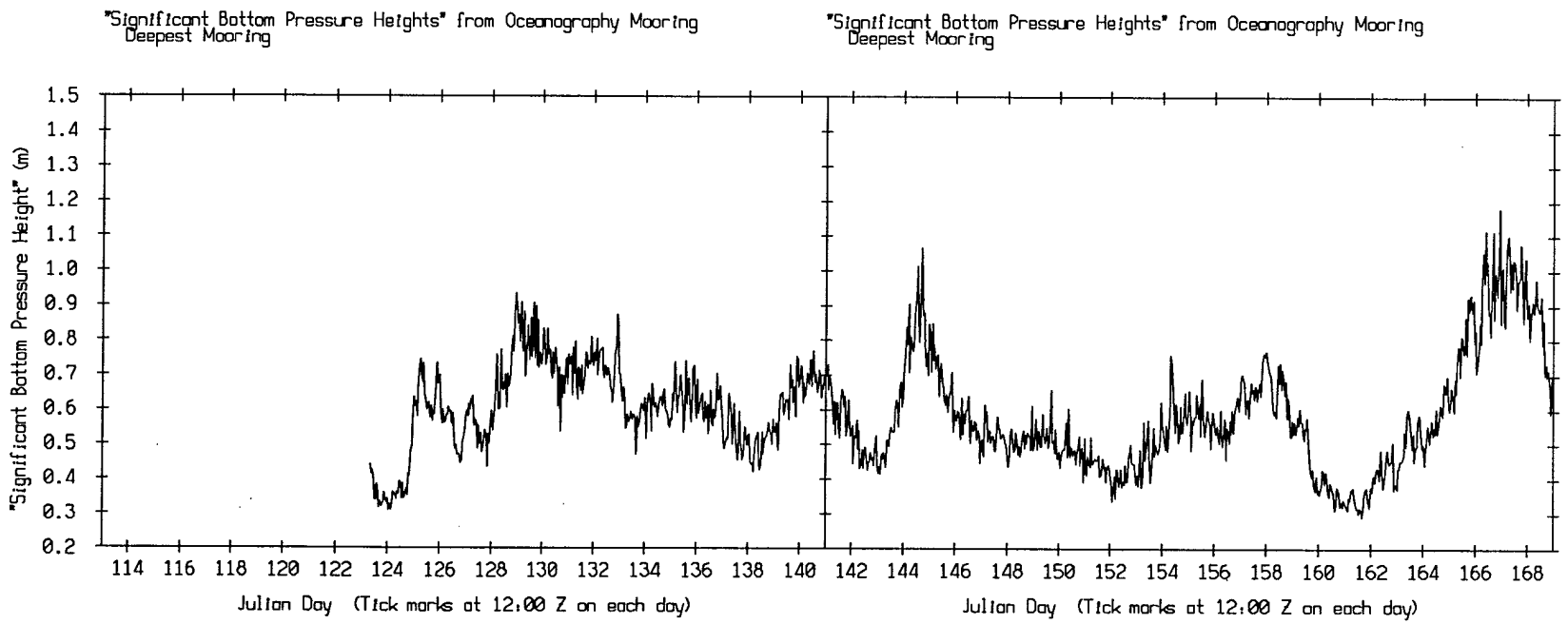
"Significant Bottom Pressure Heights" from Oceanography Mooring
Deepest Mooring
"Significant Bottom Pressure Heights" from Oceanography Mooring
Deepest Mooring
"Significant Bottom Pressure Height" (m)
1.5
1.4
1.3
1.2
1.1
1.0
0.9
0.8
0.7
0.6
0.5
0.4
0.3
0.2
114 116 118 120 122 124 126 128 130 132 134 136 138 140
142 144 146 148 150 152 154 156 158 160 162 164 166 168
Julian Day (Tick marks at 12:00 Z on each day)
Julian Day (Tick marks at 12:00 Z on each day)

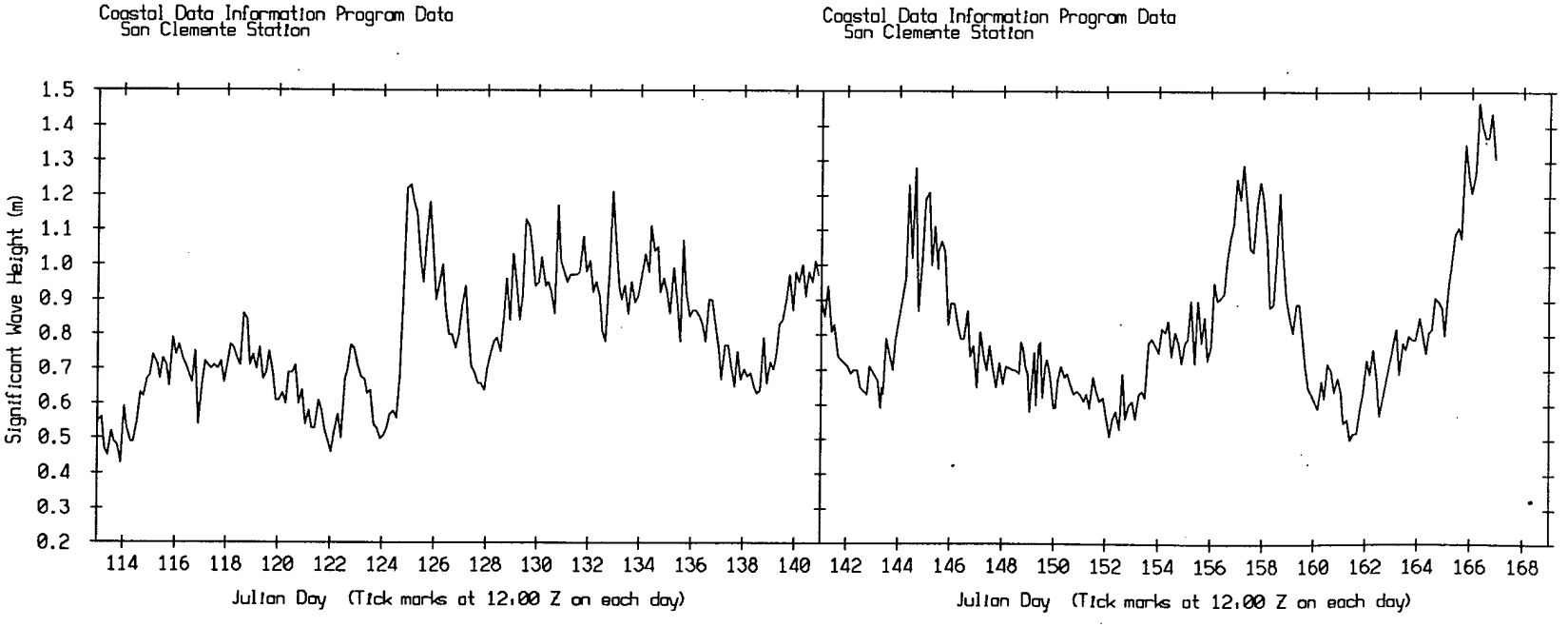
Coastal Data Information Program Data
San Clemente Station
Coastal Data Information Program Data
San Clemente Station
Significant Wave Height (m)
1.5
1.4
1.3
1.2
1.1
1.0
0.9
0.8
0.7
0.6
0.5
0.4
0.3
0.2
114 116 118 120 122 124 126 128 130 132 134 136 138 140
142 144 146 148 150 152 154 156 158 160 162 164 166 168
Julian Day (Tick marks at 12:00 Z on each day)
Julian Day (Tick marks at 12:00 Z on each day)

Figure 8

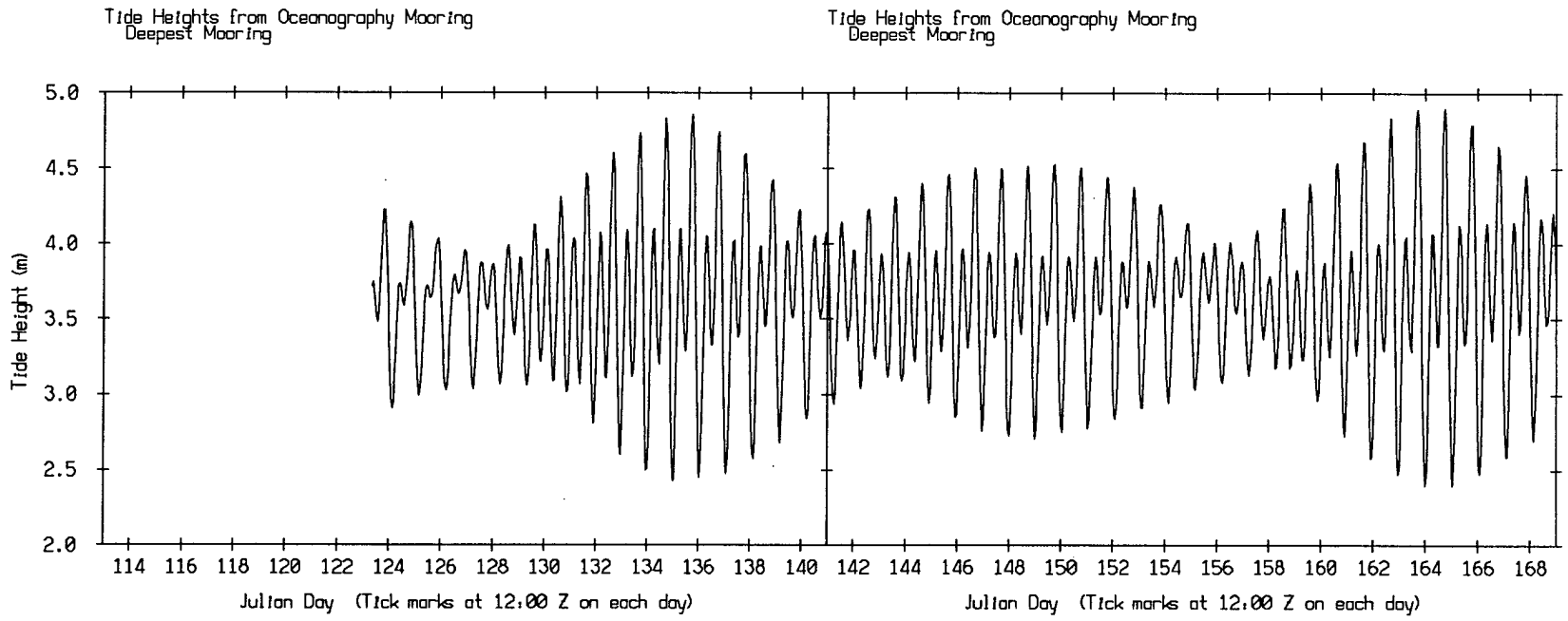
Tide Heights from Oceanography Mooring
Deepest Mooring
Tide Height (m)
5.0
4.5
4.0
3.5
3.0
2.5
2.0
114 116 118 120 122 124 126 128 130 132 134 136 138 140
Julian Day (Tick marks at 12:00 Z on each day)
Tide Heights from Oceanography Mooring
Deepest Mooring
142 144 146 148 150 152 154 156 158 160 162 164 166 168
Julian Day (Tick marks at 12:00 Z on each day)

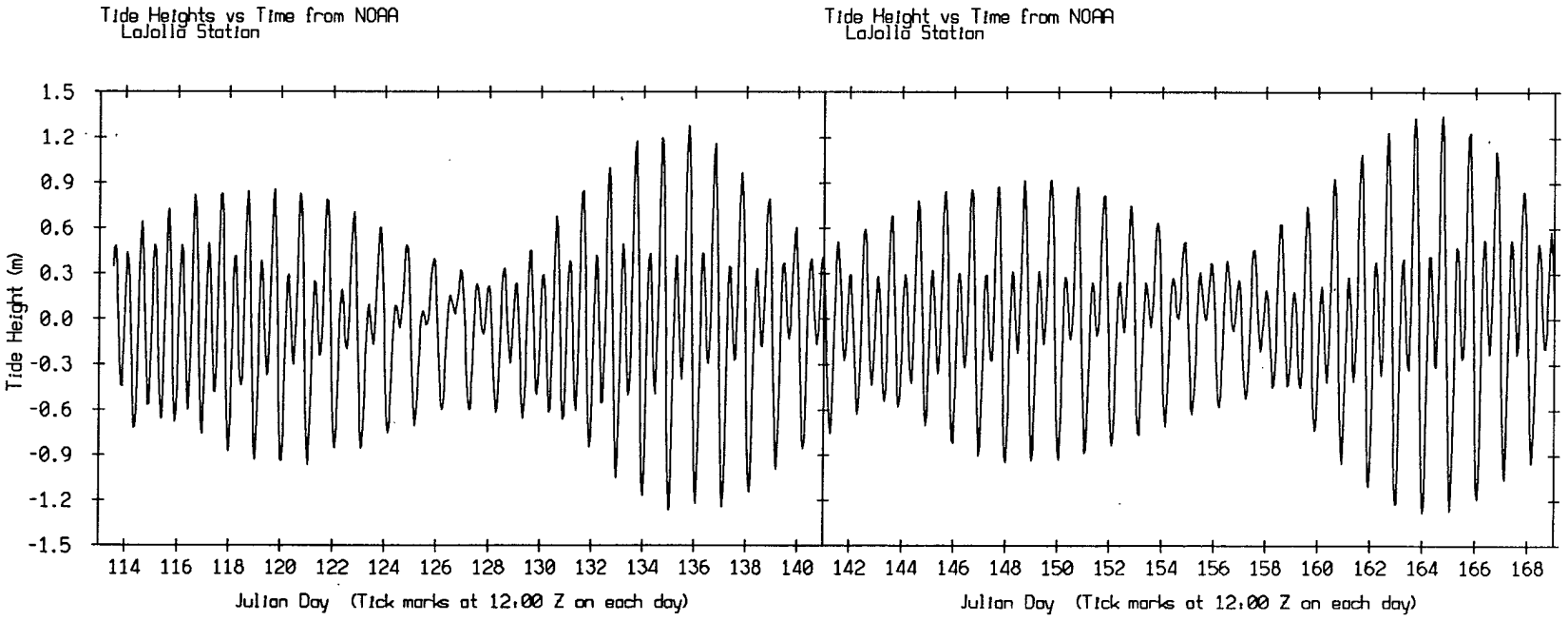
Tide Heights vs Time from NOAA
LaJolla Station
Tide Height (m)
1.5
1.2
0.9
0.6
0.3
0.0
-0.3
-0.6
-0.9
-1.2
-1.5
114 116 118 120 122 124 126 128 130 132 134 136 138 140
Julian Day (Tick marks at 12:00 Z on each day)
Tide Height vs Time from NOAA
LaJolla Station
142 144 146 148 150 152 154 156 158 160 162 164 166 168
Julian Day (Tick marks at 12:00 Z on each day)

Figure 9

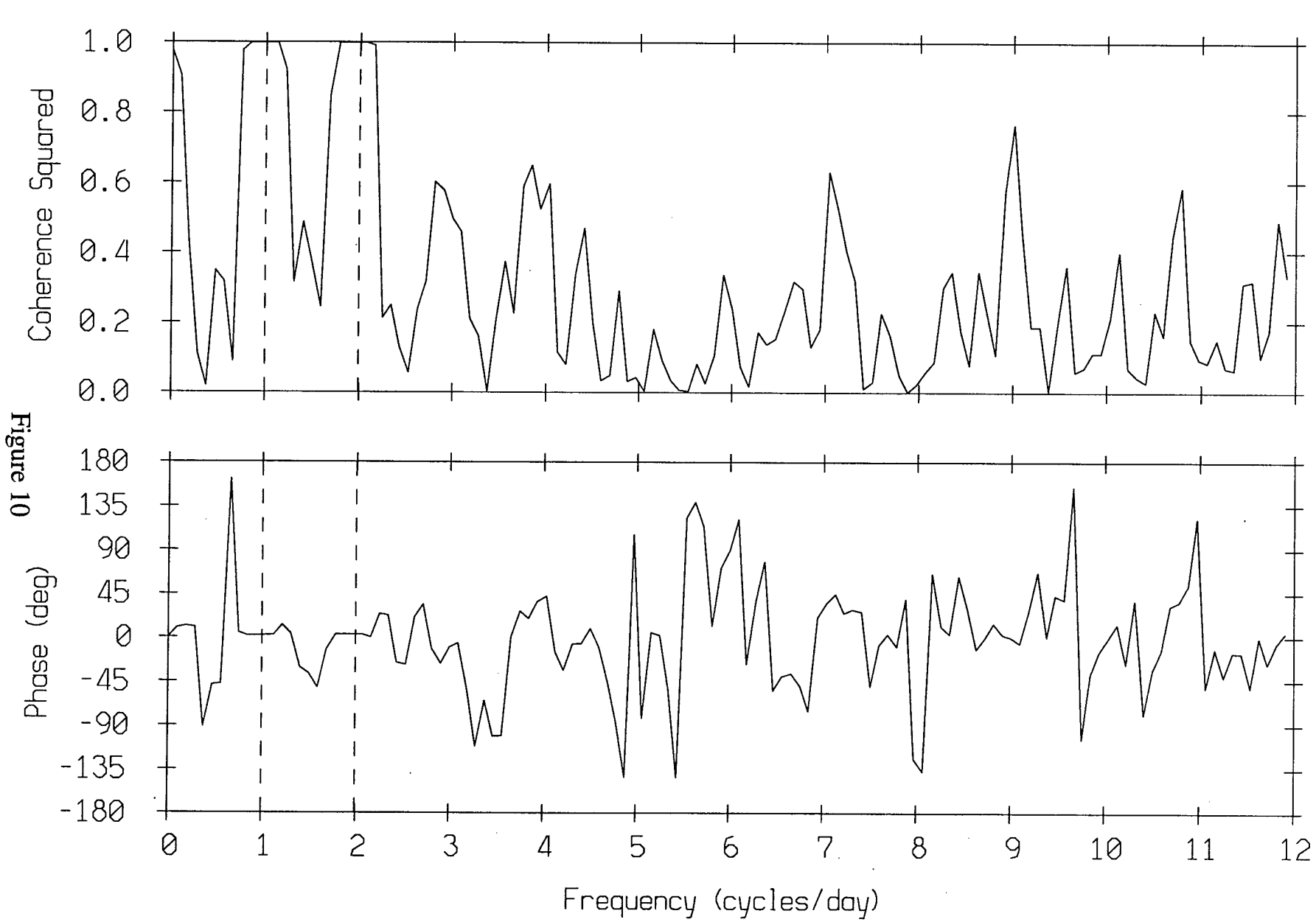
Coherence between Tide Heights at Various Stations
NOAA's La Jolla Station and the Deep Oceanography Mooring
Coherence Squared
1.0
0.8
0.6
0.4
0.2
0.0
Phase (deg)
180
135
90
45
0
-45
-90
-135
-180
0
1
2
3
4
5
6
7
8
9
10
11
12
Frequency (cycles/day)

Figure 10

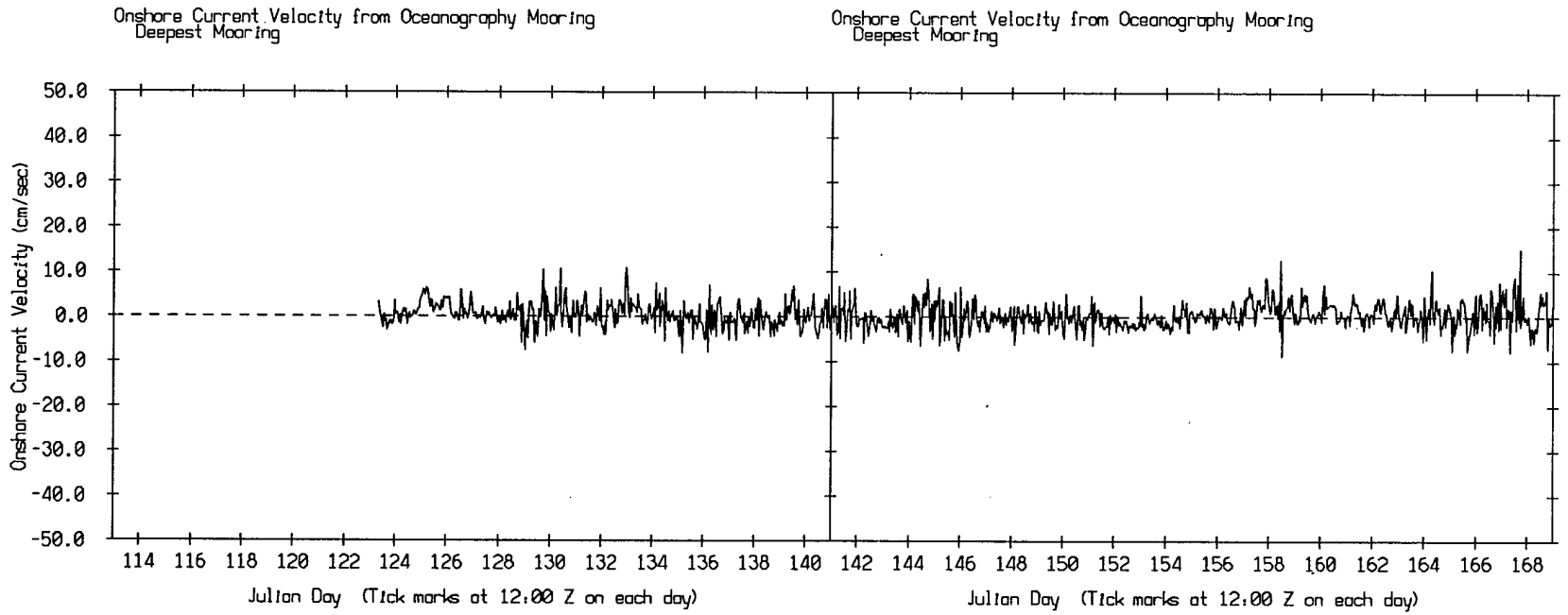
Onshore Current Velocity from Oceanography Mooring
Deepest Mooring
Onshore Current Velocity from Oceanography Mooring
Deepest Mooring
Onshore Current Velocity (cm/sec)
50.0
40.0
30.0
20.0
10.0
0.0
-10.0
-20.0
-30.0
-40.0
-50.0
114 116 118 120 122 124 126 128 130 132 134 136 138 140
142 144 146 148 150 152 154 156 158 160 162 164 166 168
Julian Day (Tick marks at 12:00 Z on each day)
Julian Day (Tick marks at 12:00 Z on each day)

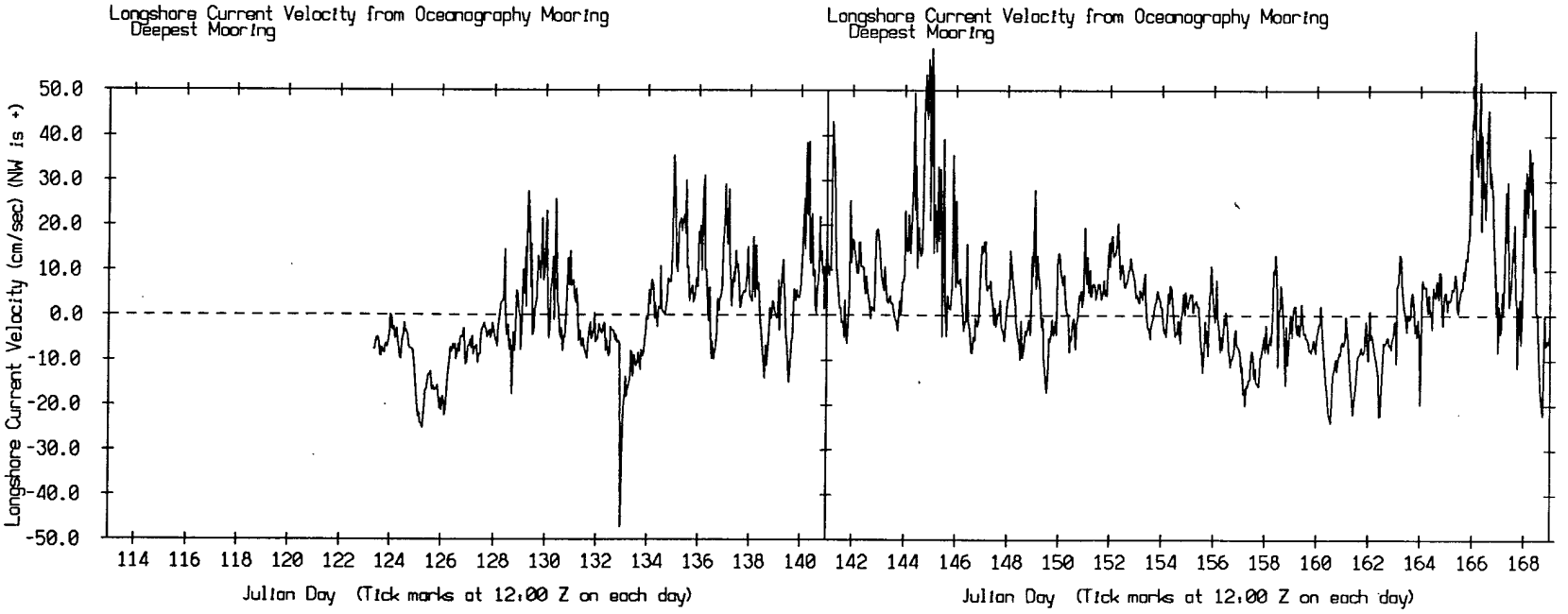
Longshore Current Velocity from Oceanography Mooring
Deepest Mooring
Longshore Current Velocity from Oceanography Mooring
Deepest Mooring
Longshore Current Velocity (cm/sec) (NW is +)
50.0
40.0
30.0
20.0
10.0
0.0
-10.0
-20.0
-30.0
-40.0
-50.0
114 116 118 120 122 124 126 128 130 132 134 136 138 140
142 144 146 148 150 152 154 156 158 160 162 164 166 168
Julian Day (Tick marks at 12:00 Z on each day)
Julian Day (Tick marks at 12:00 Z on each day)

Figure 11

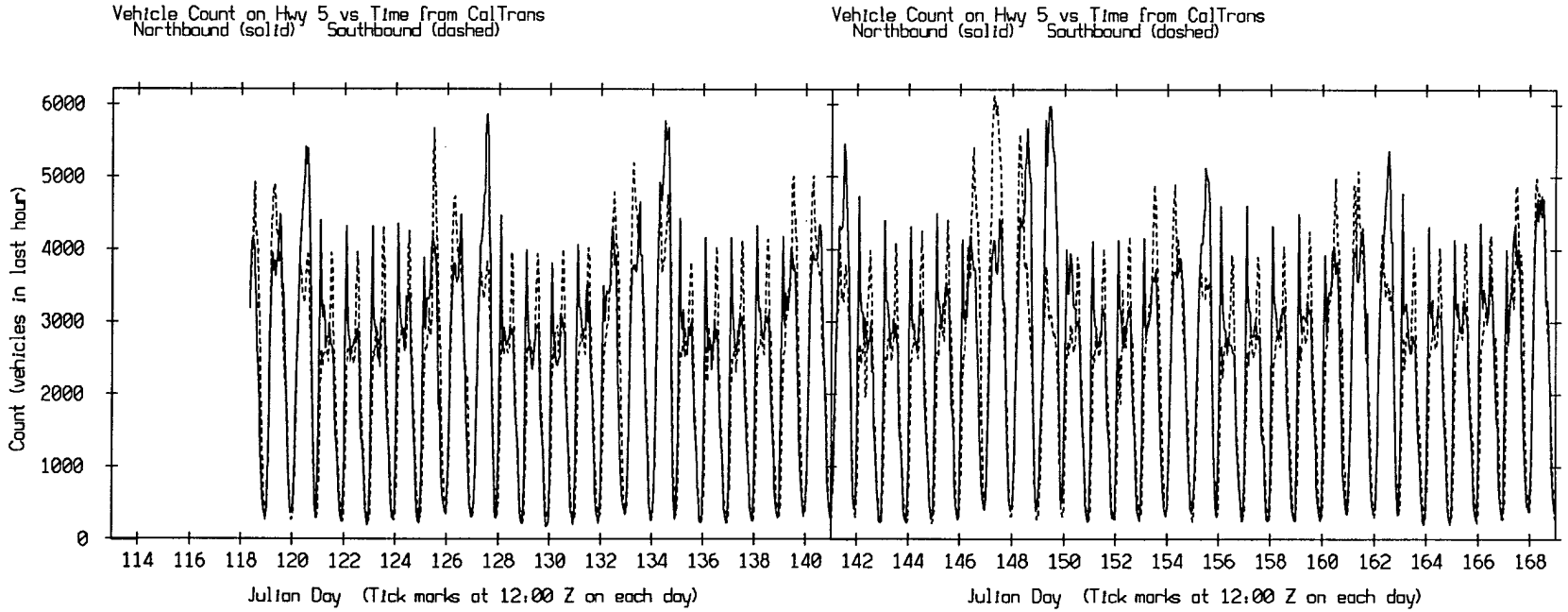
Vehicle Count on Hwy 5 vs Time from CalTrans
Northbound (solid) Southbound (dashed)
Count (vehicles in last hour)
6000
5000
4000
3000
2000
1000
0
114 116 118 120 122 124 126 128 130 132 134 136 138 140
Julian Day (Tick marks at 12:00 Z on each day)
Vehicle Count on Hwy 5 vs Time from CalTrans
Northbound (solid) Southbound (dashed)
142 144 146 148 150 152 154 156 158 160 162 164 166 168
Julian Day (Tick marks at 12:00 Z on each day)

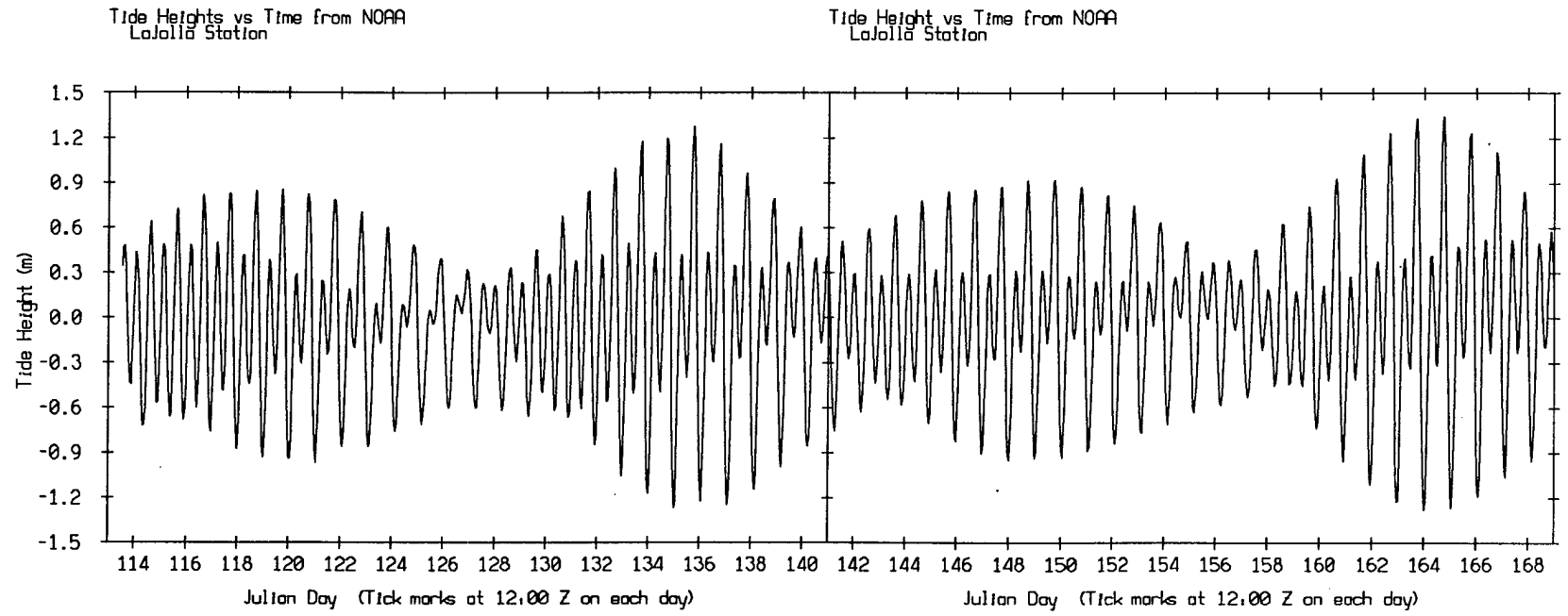
Tide Heights vs Time from NOAA
LaJolla Station
Tide Height (m)
1.5
1.2
0.9
0.6
0.3
0.0
-0.3
-0.6
-0.9
-1.2
-1.5
114 116 118 120 122 124 126 128 130 132 134 136 138 140
Julian Day (Tick marks at 12:00 Z on each day)
Tide Height vs Time from NOAA
LaJolla Station
142 144 146 148 150 152 154 156 158 160 162 164 166 168
Julian Day (Tick marks at 12:00 Z on each day)

Figure 12

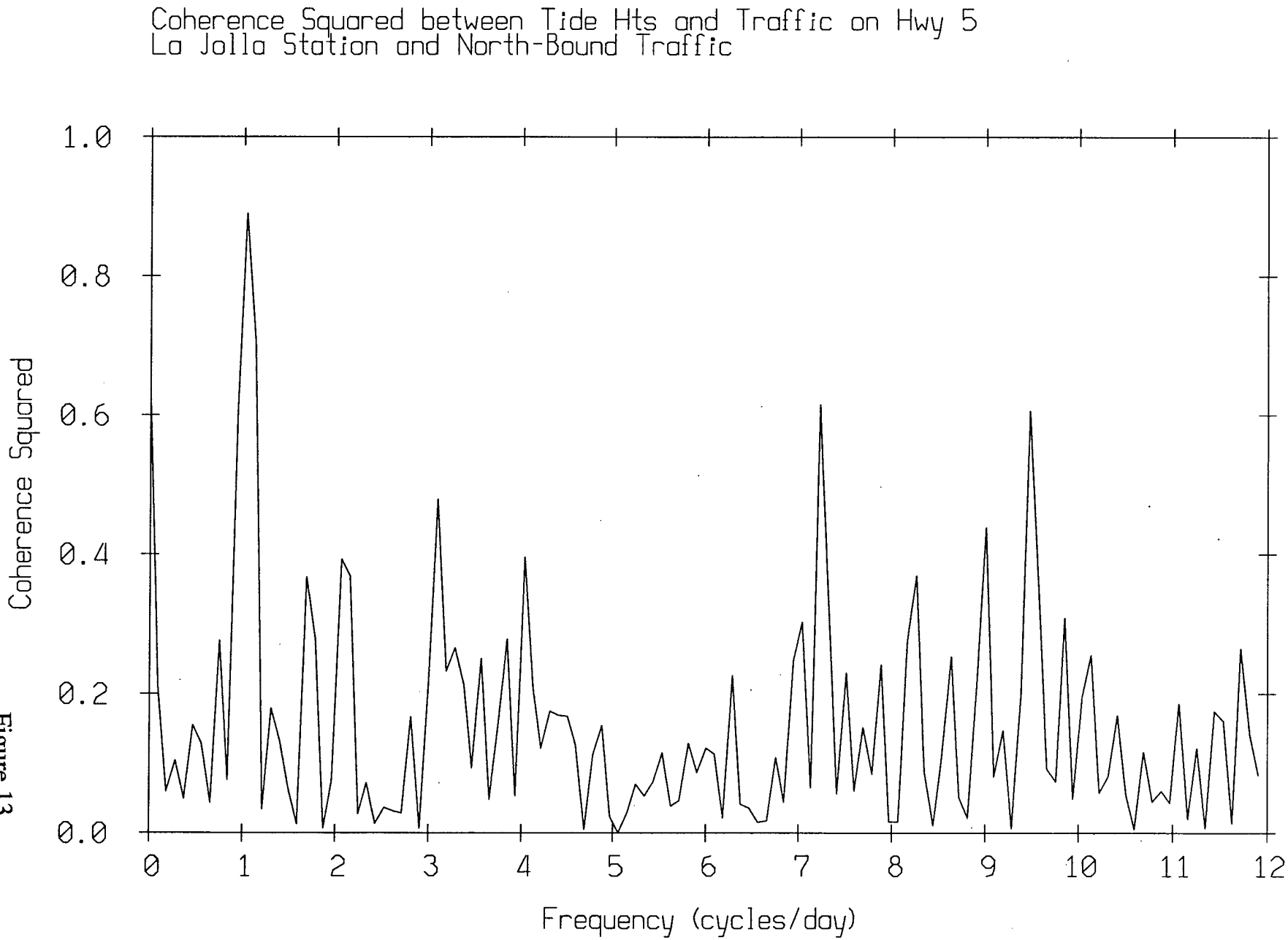
Coherence Squared between Tide Hts and Traffic on Hwy 5
La Jolla Station and North-Bound Traffic
Coherence Squared
1.0
0.8
0.6
0.4
0.2
0.0
0
1
2
3
4
5
6
7
8
9
10
11
12
Frequency (cycles/day)

Figure 13

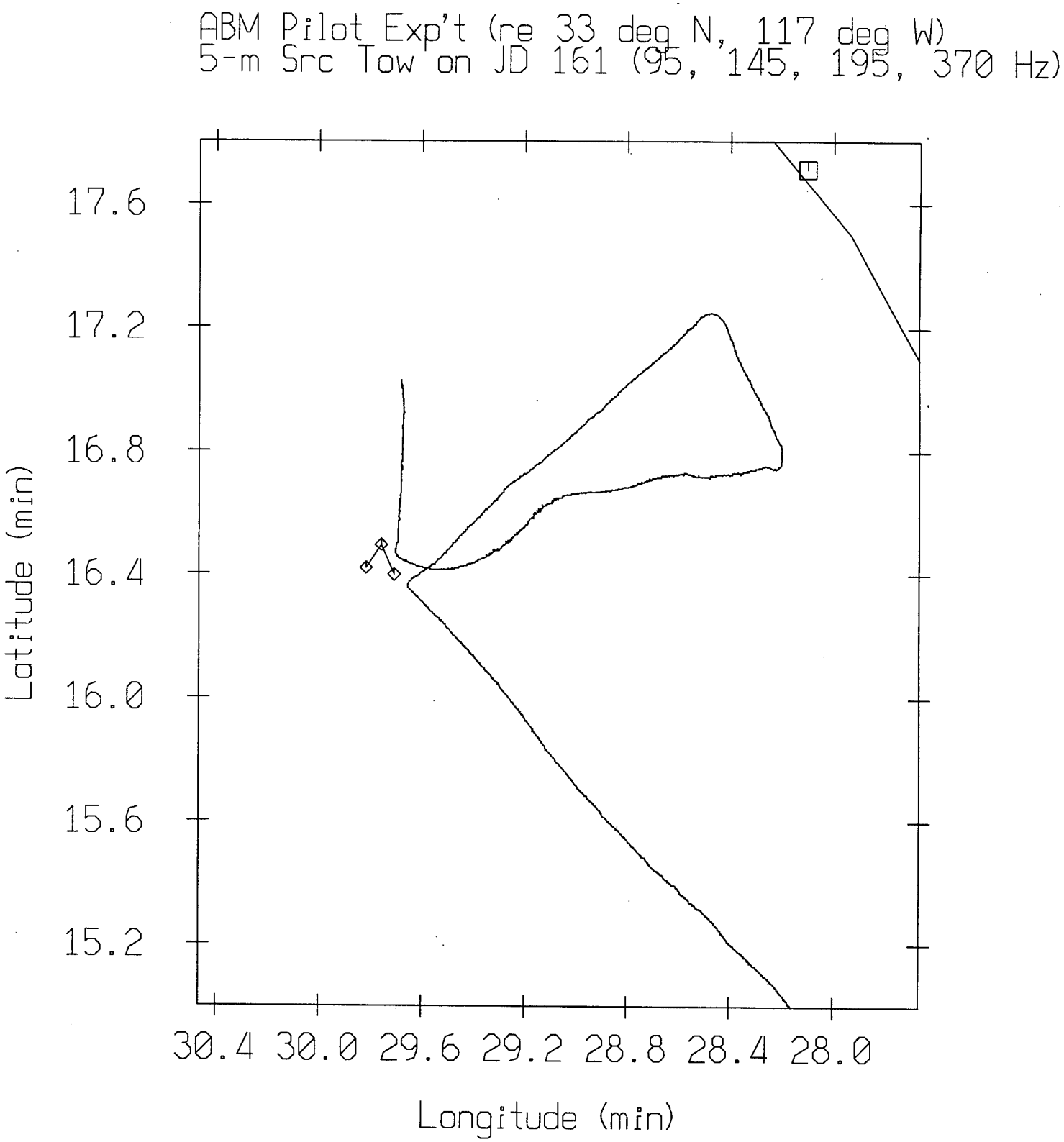
ABM Pilot Exp't (re 33 deg N, 117 deg W)
5-m Src Tow on JD 161 (95, 145, 195, 370 Hz)
17.6
17.2
16.8
16.4
16.0
15.6
15.2
Latitude (min)
30.4 30.0 29.6 29.2 28.8 28.4 28.0
Longitude (min)

Figure 14

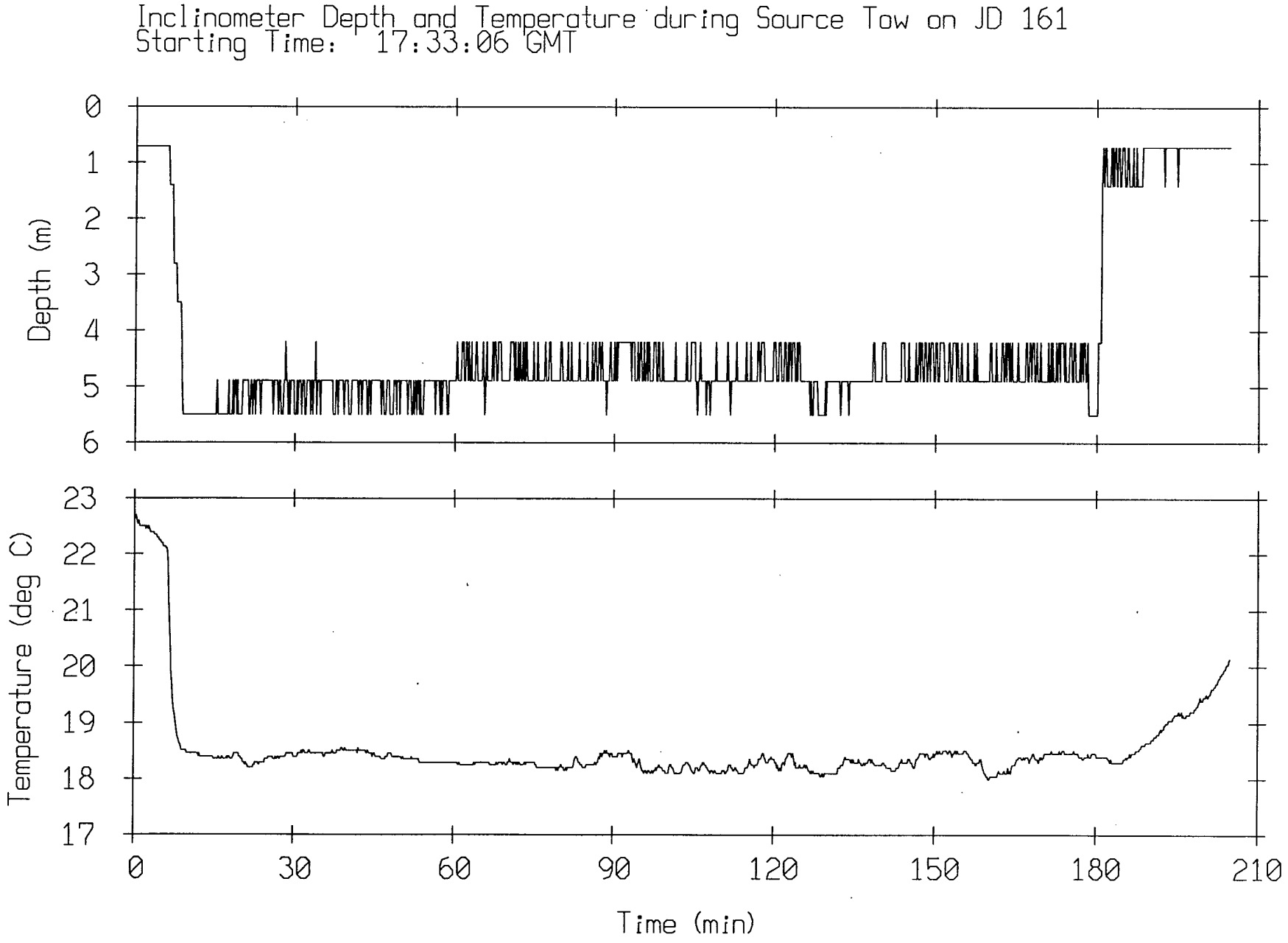
Inclinometer Depth and Temperature during Source Tow on JD 161
Starting Time: 17:33:06 GMT
Depth (m)
0
1
2
3
4
5
6
Temperature (deg C)
23
22
21
20
19
18
17
0
30
60
90
120
150
180
210
Time (min)

Figure 15

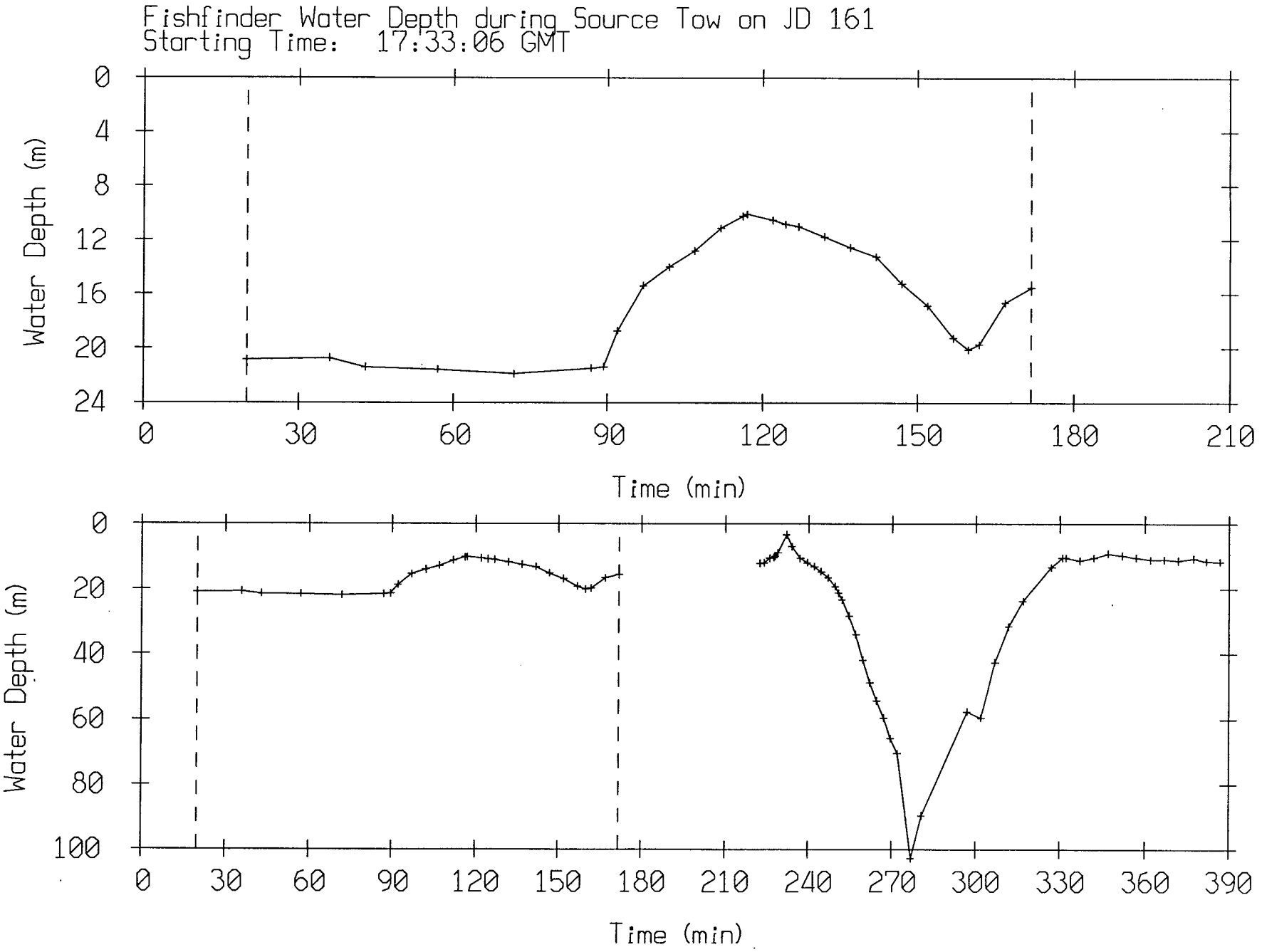
Fishfinder Water Depth during Source Tow on JD 161
Starting Time: 17:33:06 GMT
Water Depth (m)
0
4
8
12
16
20
24
0
30
60
90
120
150
180
210
Time (min)
Water Depth (m)
0
20
40
60
80
100
0
30
60
90
120
150
180
210
240
270
300
330
360
390
Time (min)

Figure 16

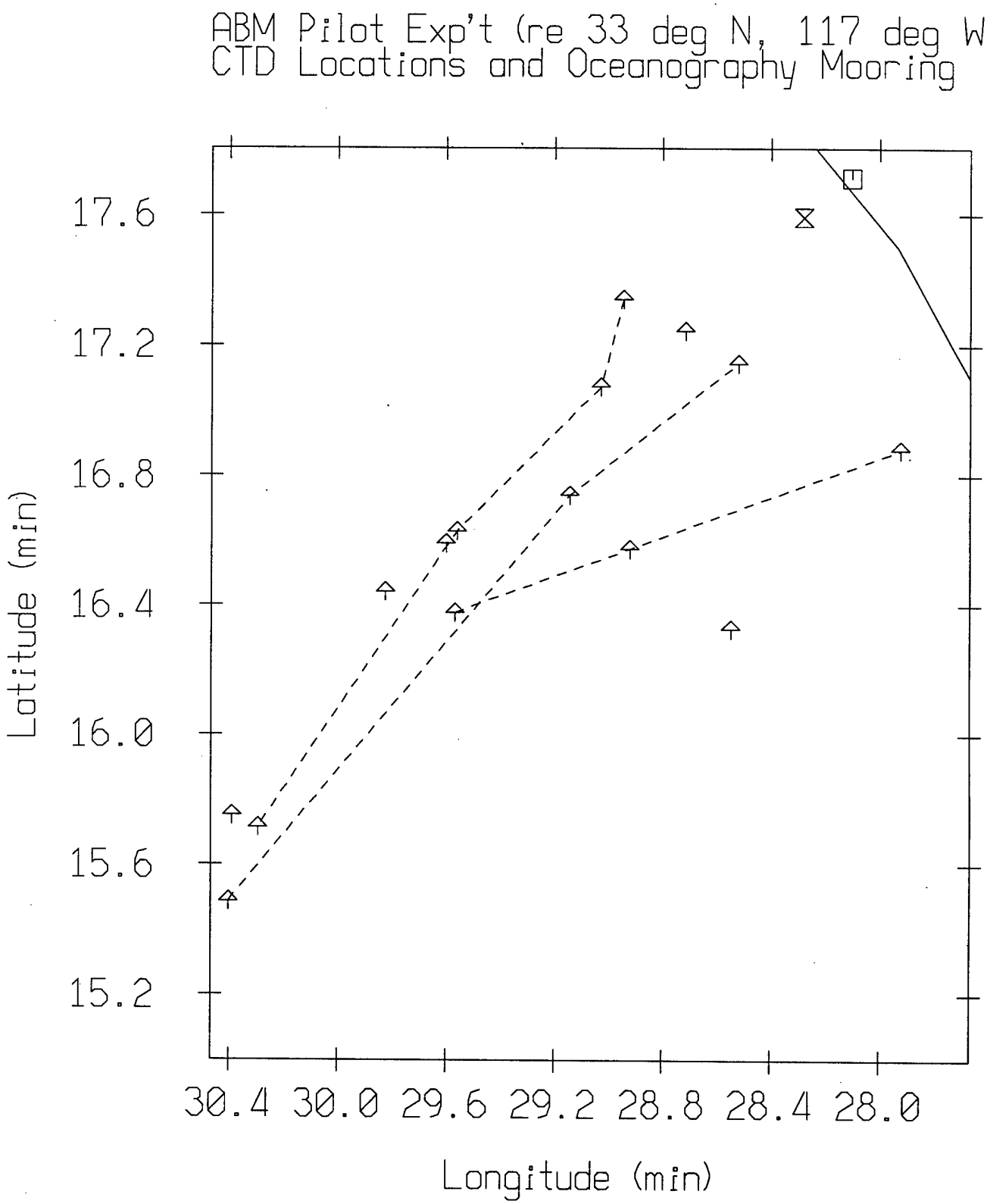
ABM Pilot Exp't (re 33 deg N, 117 deg W)
CTD Locations and Oceanography Mooring
17.6
17.2
16.8
16.4
16.0
15.6
15.2
Latitude (min)
30.4 30.0 29.6 29.2 28.8 28.4 28.0
Longitude (min)

Figure 17

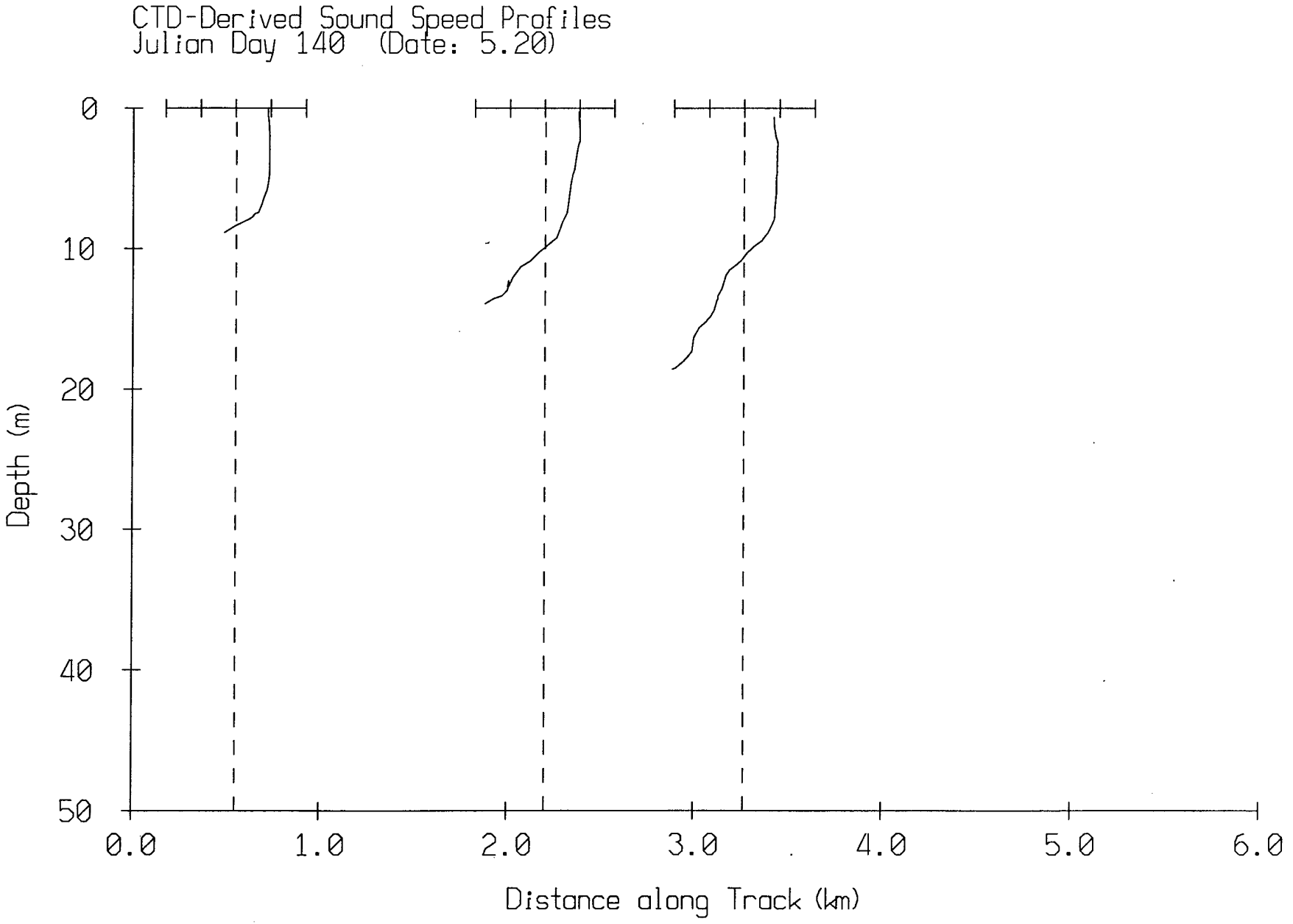
CTD-Derived Sound Speed Profiles
Julian Day 140 (Date: 5.20)
Depth (m)
0
10
20
30
40
50
0.0
1.0
2.0
3.0
4.0
5.0
6.0
Distance along Track (km)

Figure 18

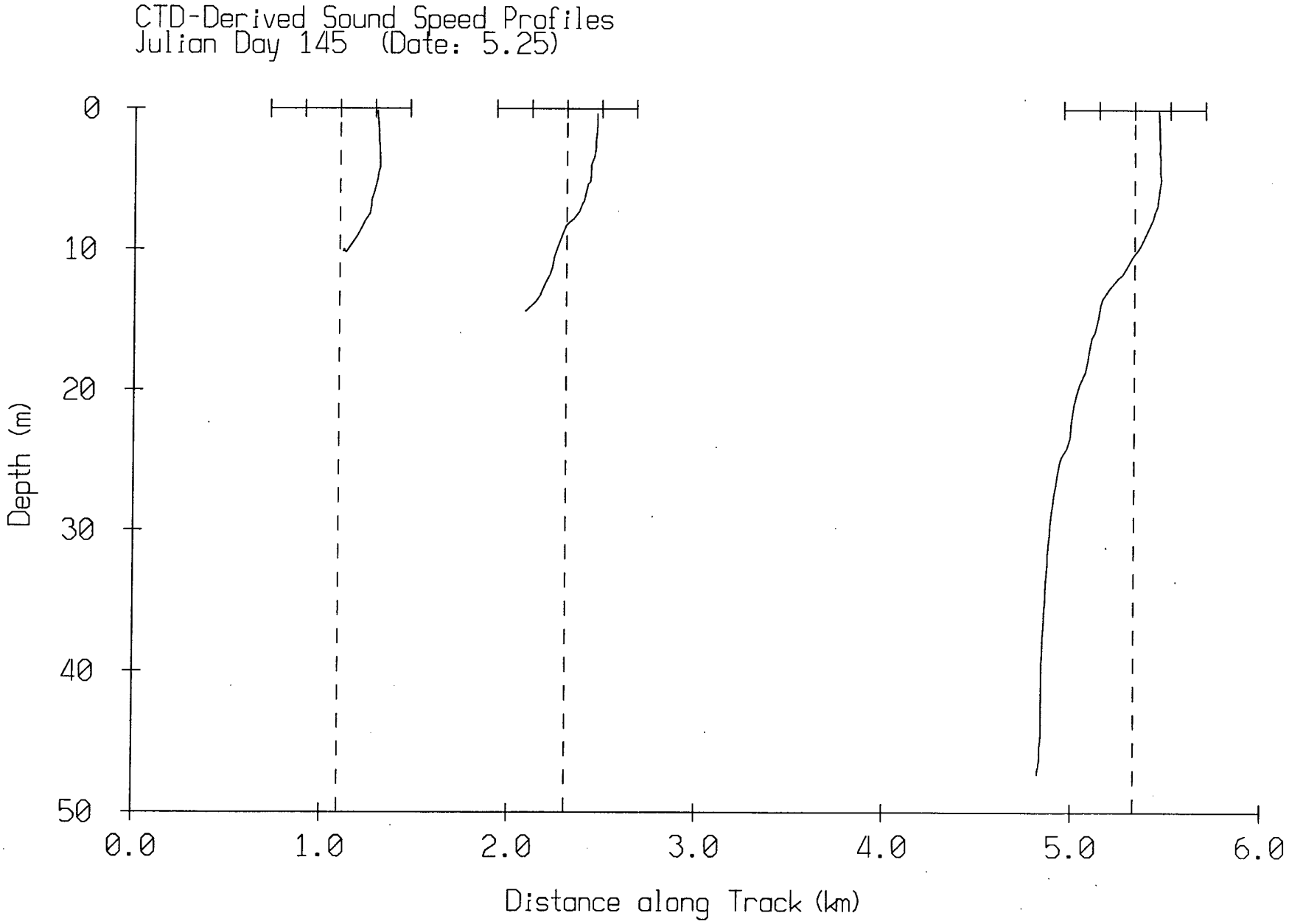
CTD-Derived Sound Speed Profiles
Julian Day 145 (Date: 5.25)
Depth (m)
0
10
20
30
40
50
0.0
1.0
2.0
3.0
4.0
5.0
6.0
Distance along Track (km)

Figure 19

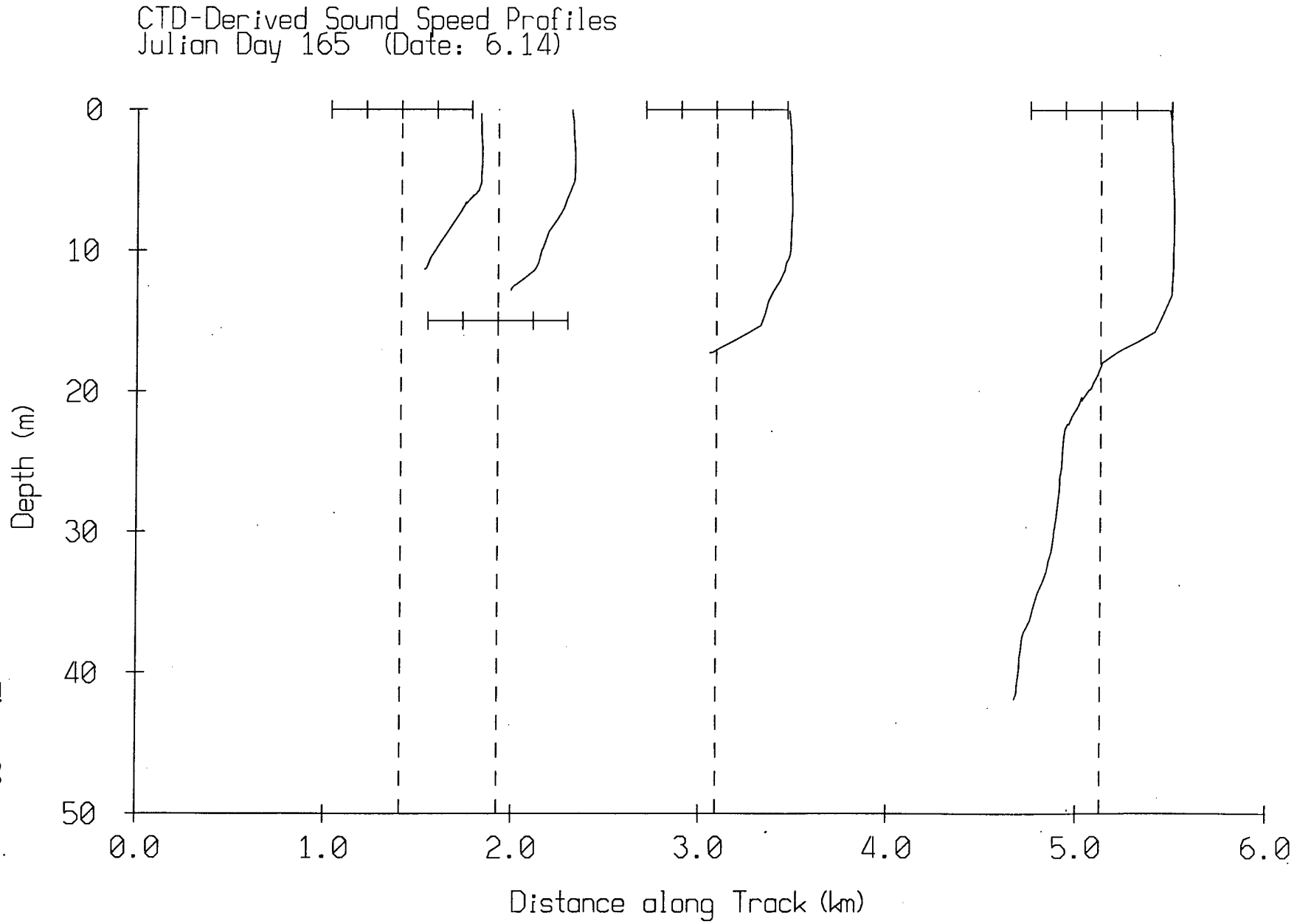
CTD-Derived Sound Speed Profiles
Julian Day 165 (Date: 6.14)
Depth (m)
0
10
20
30
40
50
0.0
1.0
2.0
3.0
4.0
5.0
6.0
Distance along Track (km)

Figure 20

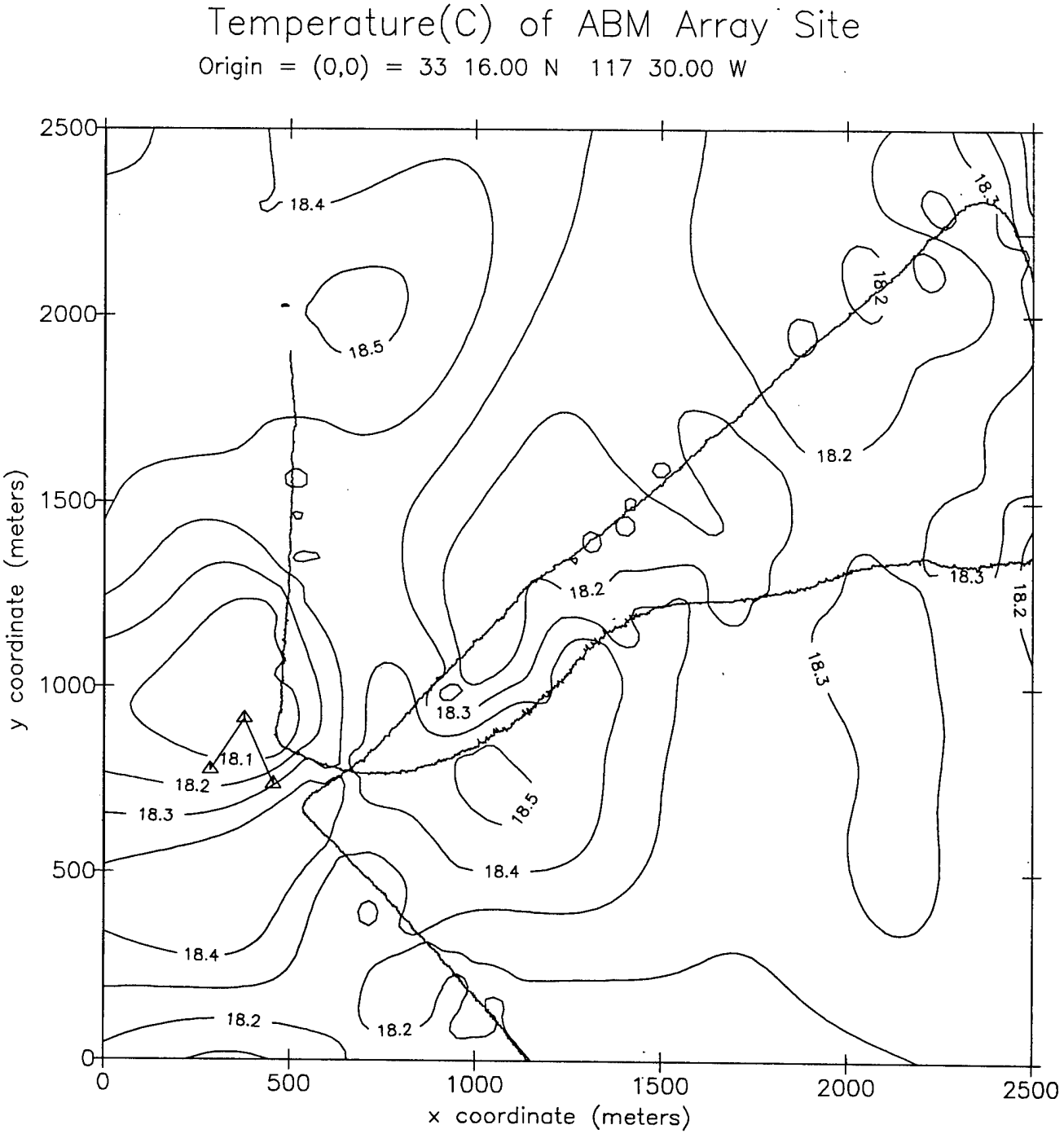
Temperature(C) of ABM Array Site
Origin = (0,0) = 33 16.00 N 117 30.00 W
y coordinate (meters)
x coordinate (meters)
0
500
1000
1500
2000
2500
18.1
18.2
18.3
18.4
18.5

Figure 21

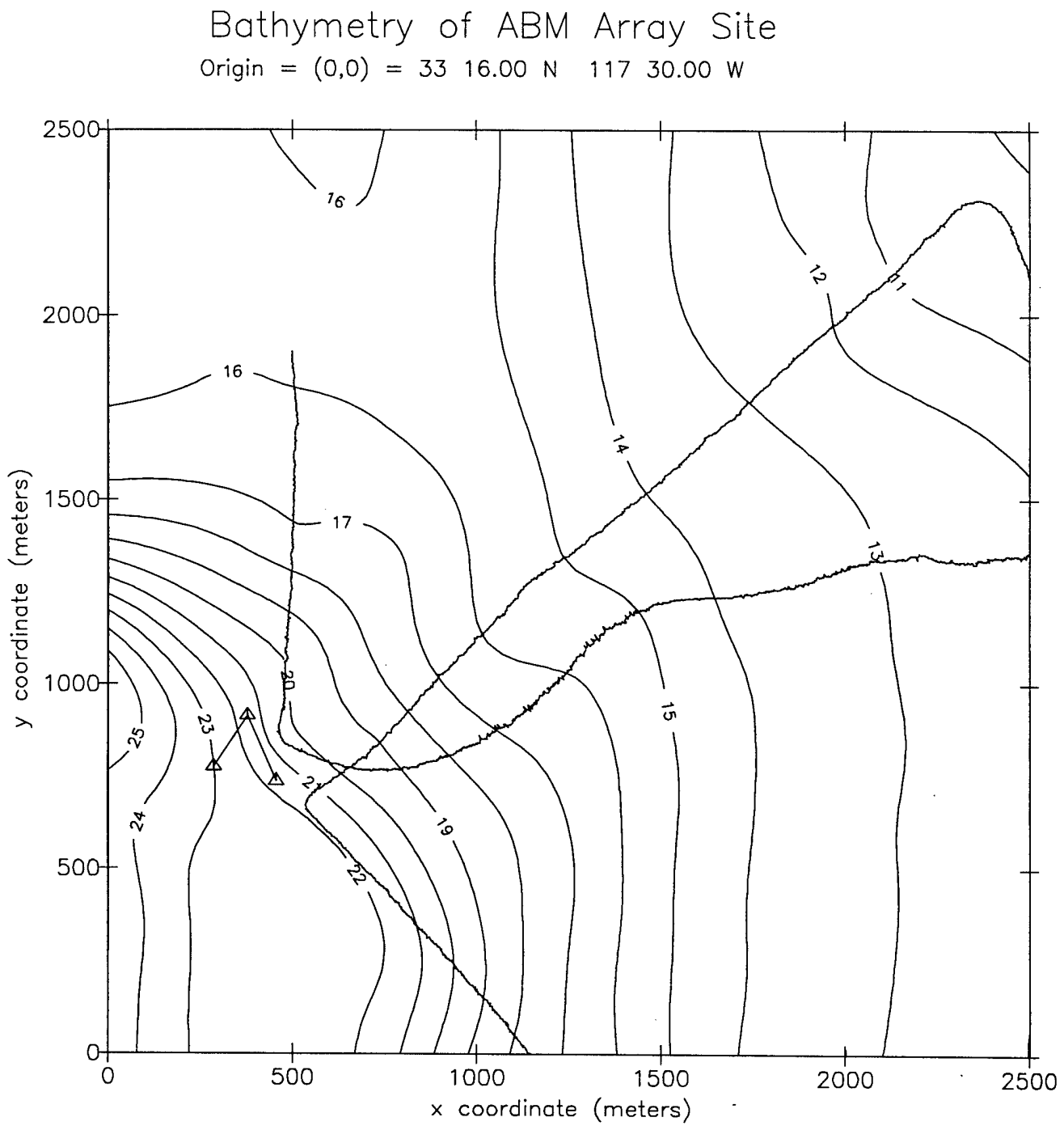
Bathymetry of ABM Array Site
Origin = (0,0) = 33 16.00 N 117 30.00 W
y coordinate (meters)
x coordinate (meters)
0
500
1000
1500
2000
2500
16
17
20
25
23
21
24
22
19
15
14
13
12
11

Figure 22

ONR/MPL REPORT DISTRIBUTION

Chief of Naval Research (3)
Ballston Centre Tower One
800 North Quincy Street
Arlington, VA 22217-5660
Attn: Dr. Richard Doolittle
Code 321US

Regional Director (1)
ONR Detachment
San Diego Regional Office
4520 Executive Drive, Suite 300
San Diego, CA 92121-3019

Commanding Officer (1)
Naval Research Laboratory
4555 Overlook Avenue, S.W.
Attn: Code 2627
Washington, D.C. 20375-5320

Defense Technical Information Center (4)
8725 John J. Kingman Road
Suite 0944
Ft Belvoir, VA 22060-6218